

Basolateral Amygdala Astrocytes Are Engaged by the Acquisition and Expression of a Contextual Fear Memory

 **Rebecca L. Suthard**,^{1,4*}  **Ryan A. Senne**,^{1,4*} **Michelle D. Buzharsky**,² **Angela Y. Pyo**,⁴  **Kaitlyn E. Dorst**,^{1,4} **Anh H. Diep**,² **Rebecca H. Cole**,² and **Steve Ramirez**^{3,4}

¹Graduate Program for Neuroscience, Boston University, Boston, Massachusetts 02215, ²Undergraduate Program in Neuroscience, Boston University, Boston, Massachusetts 02215, ³Department of Biomedical Engineering, Boston University, Boston, Massachusetts 02215, and

⁴Department of Psychological and Brain Sciences, Center for Systems Neuroscience, Neurophotonics Center, and Photonics Center, Boston University, Boston, Massachusetts 02215

Astrocytes are key cellular regulators within the brain. The basolateral amygdala (BLA) is implicated in fear memory processing, yet most research has entirely focused on neuronal mechanisms, despite a significant body of work implicating astrocytes in learning and memory. In the present study, we used *in vivo* fiber photometry in C57BL/6J male mice to record from amygdalar astrocytes across fear learning, recall, and three separate periods of extinction. We found that BLA astrocytes robustly responded to foot shock during acquisition, their activity remained remarkably elevated across days in comparison to unshocked control animals, and their increased activity persisted throughout extinction. Further, we found that astrocytes responded to the initiation and termination of freezing bouts during contextual fear conditioning and recall, and this behavior-locked pattern of activity did not persist throughout the extinction sessions. Importantly, astrocytes do not display these changes while exploring a novel context, suggesting that these observations are specific to the original fear-associated environment. Chemogenetic inhibition of fear ensembles in the BLA did not affect freezing behavior or astrocytic calcium dynamics. Overall, our work presents a real-time role for amygdalar astrocytes in fear processing and provides new insight into the emerging role of these cells in cognition and behavior.

Key words: amygdala; astrocytes; calcium; fear; learning; memory

Significance Statement

We show that basolateral amygdala astrocytes are robustly responsive to negative experiences, like shock, and display changed calcium activity patterns through fear learning and memory. Additionally, astrocytic calcium responses become time locked to the initiation and termination of freezing behavior during fear learning and recall. We find that astrocytes display calcium dynamics unique to a fear-conditioned context, and chemogenetic inhibition of BLA fear ensembles does not have an impact on freezing behavior or calcium dynamics. These findings show that astrocytes play a key real-time role in fear learning and memory.

Introduction

Memory acquisition, recall, and extinction are critical phases for information processing in the brain; disruption of any of these processes can lead to pathologic states of cognition and behavior. Fear memories are one of the most well-studied forms of memory and have been shown to recruit numerous brain areas including the hippocampus and basolateral amygdala (BLA). Specifically, during pavlovian fear conditioning (FC), the CA1 and CA3 subregions of the hippocampus (HPC) relay information to the amygdala via the ventroangular pathway or through the entorhinal cortex, which also projects to the prefrontal cortex. The amygdala then is thought to send output to the central amygdala, which in turn sends output to the lateral hypothalamus or periaqueductal gray to alter the sympathetic nervous system and gate freezing behavior, respectively. This complex

Received Sep. 16, 2022; revised May 11, 2023; accepted May 18, 2023.

Author contributions: R.L.S., R.A.S., M.D.B., R.H.C., and S.R. designed research; R.L.S., R.A.S., M.D.B., A.Y.P., K.E.D., A.H.D., and R.H.C. performed research; R.L.S., R.A.S., M.D.B., A.Y.P., and S.R. analyzed data; R.L.S., R.A.S., and S.R. wrote the paper.

This work is supported by the NIH Early Independence Award DP5 OD023106-01, NIH Transformative Award, Brain and Behavior Research Foundation Young Investigator Grant, McKnight Foundation Memory and Cognitive Disorders Award, Pew Scholars Program in the Biomedical Sciences, Air Force Office of Scientific Research Grant FA9550-21-1-0310, and Center for Systems Neuroscience and Neurophotonics Center at Boston University.

*R.L.S. and R.A.S contributed equally to this work.

The authors declare no competing financial interests.

Correspondence should be addressed to Steve Ramirez at dvsteve@bu.edu.

<https://doi.org/10.1523/JNEUROSCI.1775-22.2023>

Copyright © 2023 the authors

fear circuitry is necessary for proper memory processing, and these regions each differentially contribute to the behavioral expression of fear.

Previous work has demonstrated the active involvement of astrocytes in cognition and behavior by regulating synaptic plasticity, supporting metabolic homeostasis, modulating neurotransmitter action, and releasing their own gliotransmitters to exert wide-ranging effects on the brain (Parpura et al., 1994; Porter and McCarthy, 1997; Araque et al., 1999, 2001; Bezzi and Volterra, 2001; Haydon, 2001; Fellin et al., 2004; Koizumi et al., 2005; Perea and Araque, 2005; Volterra and Meldolesi, 2005; Perea et al., 2009; Di Castro et al., 2011; Araque et al., 2014; Covelo and Araque, 2018; Durkee et al., 2019). Broadly, chemogenetic and optogenetic perturbations of astrocytic functioning have been shown to impair or enhance both recent and remote memory in the hippocampus, amygdala, and prefrontal cortex (Liao et al., 2017; Martin-Fernandez et al., 2017; Adamsky et al., 2018; Kol et al., 2020; Li et al., 2020; Fan et al., 2021). The effects of these manipulations depend heavily on the brain region of interest, the signaling pathways perturbed, and the time point of manipulation during behavior. Mounting evidence suggests that astrocytes may modulate local and projection-specific network activity in memory processes (Kol et al., 2020; Martin-Fernandez et al., 2017). For example, an earlier study demonstrated that hippocampal dorsal CA1 (dCA1) astrocytic Gq activation during contextual fear conditioning (CFC) is sufficient to promote long-term potentiation and enhance subsequent recall in mice, whereas neuronal activation does not (Adamsky et al., 2018). Further research in the BLA has shown that fear conditioning itself downregulates astrocytic Rac1 to facilitate the formation of a conditioned fear memory (Liao et al., 2017; Fan et al., 2021). Additionally, BLA astrocytic Gq pathway activation during fear conditioning increased auditory memory, but not contextual memory retrieval, dissociating the role of these cells in multiple types of aversive learning (Lei et al., 2022). Finally, Gq activation of astrocytes in the BLA after cued fear extinction training decreases freezing levels during extinction recall 24 h later (Shelkar et al., 2021). This evidence supports bidirectional astrocyte–neuron communication in multiple subdivisions of the amygdala and suggests their active control over the functional connectivity of the amygdala with other canonical fear-learning hubs.

Despite the recent interest in astrocytic contributions to memory, these studies predominantly use perturbation approaches (e.g., cell-type-specific activation or inhibition of cellular activity), whereas neuronal investigations may now multiplex these causal approaches with optical imaging to gain real-time insight on cellular activity during behavior. Still, there are relatively few studies using these approaches, even with newer genetically encoded calcium indicators (GECIs) and transgenic mouse lines that are capable of preferentially targeting astrocytes for dynamic calcium recordings across behavior (Corkrum et al., 2020; Lines et al., 2020; Qin et al., 2020; Tsunematsu et al., 2021; Lin et al., 2022). Understanding the activity of astrocytes in real time is essential for understanding cognition, especially given that the brain predominantly consists of glia.

The BLA is a key hub for valence-specific memories. Prior work has shown that the BLA is necessary for the encoding and retrieval of the emotional component of fearful experiences, and lesioning experiments have shown that its disruption strongly inhibits proper emotional responses (Maren et al., 1996; Maren, 1999; Zhang and Li, 2018). Furthermore, the BLA has also been shown to be necessary for the acquisition and extinction of

contextual fear memory in mice, suggesting it plays a key role in every stage of fear learning. Despite the relatively large body of literature implicating the BLA in fear conditioning, almost all this work has focused on neuronal responses, and there is currently a limited understanding on how astrocytic calcium responses in the BLA manifest across fear acquisition, recall, and contextual extinction. Furthermore, previous work suggests that perturbation of BLA neurons during fear recall is capable of diminishing freezing behaviors (Han et al., 2009; Redondo et al., 2014; Gore et al., 2015; Liu et al., 2022), although coupled activity at the astrocyte–neuron interface remains relatively understudied activity.

To address this, we use freely moving fiber photometry (Cui et al., 2014; Gunaydin et al., 2014) to record population-level astrocytic calcium dynamics across the classic CFC paradigm. First, we find that astrocytes in the BLA are shock responsive, which suggests that astrocytes in this amygdalar subregion process salient and/or aversive-related stimuli. Next, we find that astrocytes in the shock condition displayed unique calcium events across fear learning compared with the unshocked control group. Then we observed calcium perievents at the initiation and termination of freezing bouts during recall, but this did not persist into extinction sessions. We then used activity-dependent and chemogenetic-mediated inhibition of BLA cells to determine whether this affected animal behavior and/or astrocytic signaling, and we found no change in freezing or real-time dynamics. Finally, astrocytic changes were associated with the fear-conditioned environment, as in a novel context we observed no differences in exploratory behaviors nor any changes in calcium event characteristics across the shock and no-shock groups.

Together, our experiments provide a more comprehensive understanding of the contributions of glial cells to learning and memory processes. Perturbation of these cells during extinction memory formation and maintenance may pave the way for more successful therapeutic interventions in humans with disorders of maladaptive fear learning, such as post-traumatic stress disorder.

Materials and Methods

Animals

Wild-type male C57BL/6J mice [prenatal day (P)29–35; weight 17–19 g; Charles River Laboratories] were housed in groups of four to five mice per cage. The animal facilities (vivarium and behavioral testing rooms) were maintained on a 12 h light cycle (0700–1900). Mice received food and water *ad libitum* before and after surgery. Following surgery, mice were group housed with littermates and allowed to recover for 3 weeks before experimentation. All subjects were treated in accord with Protocol 201800579 approved by the Institutional Animal Care and Use Committee at Boston University.

Stereotaxic surgery

For all surgeries, mice were anesthetized with 3.0% isoflurane inhalation during induction and maintained at 1–2% isoflurane inhalation through stereotaxic nose cone delivery (oxygen 1 l/min). Ophthalmic ointment was applied to the eyes to provide adequate lubrication and prevent corneal desiccation. The hair on the scalp above the surgical site was removed using Veet hair removal cream and subsequently cleaned with alternating applications of betadine solution and 70% ethanol; 2.0% lidocaine hydrochloride was injected subcutaneously as local analgesia before midsagittal incision of the scalp skin to expose the skull, and a 0.1 mg/kg (5 mg/ml) subcutaneous dose of meloxicam and 0.1–0.2 ml of sterile saline were administered at the beginning of surgery. For fiber photometry implant surgeries, animals received a unilateral craniotomy with a 0.5–0.6 mm drill bit for BLA injections. A 10 μ l airtight Hamilton syringe with an attached 33 gauge beveled needle was slowly lowered to the following coordinates of BLA: −1.40 anteroposterior, −3.20

mediolateral, and -4.80 dorsoventral. All coordinates are given relative to bregma (millimeters). A volume of 500 nl of adeno-associated virus (AAV)-GfaABC1D-cyto-GCaMP6f-SV40 (Penn Vector Core) was injected at 50 nl/min using a microinfusion pump for the BLA coordinates (UltraMicroPump III, World Precision Instruments). After the injection was complete, the needle remained at the target site for 5–7 min postinjection before removal. Following viral injection, a unilateral optic fiber (200 μ m core diameter, 1.25 mm ferrule diameter) was implanted at the site of injection. The implant was secured to the skull with a layer of adhesive cement (Parkell, C&M Metabond) followed by multiple layers of dental cement (Stoelting). Following surgery, mice were injected with a 0.1 mg/kg intraperitoneal dose of buprenorphine for pain management. They were placed in a recovery cage with a heating pad on medium heat until fully recovered from anesthesia. To allow for recovery and viral expression, we waited 3 weeks before beginning our behavioral paradigm. Histologic assessment verified viral targeting, and data from off-target injections were not included in further analyses.

For activity-dependent (engram) virus surgeries, mice were placed on a doxycycline (Dox) diet for 72 h before surgery. The same injection, viral volume, and fiber photometry implantation methods were used as described above, with the addition of 200–250 nl AAV9-c-fos-tTA-TRE-hM4Di-mCherry or AAV9-c-fos-tTA-TRE-mCherry virus in bilateral BLA to allow for inhibition of the neuronal fear engram during recall.

Fiber photometry

A 470 nm LED (FP3002, Neurophotometrics) delivered an excitation wavelength of light to astrocytes expressing GCaMP6f via a single fiber optic implant. The emitted 530 nm signal from the indicator was collected via this same fiber, spectrally separated using a dichroic mirror, passed through a series of filters, and was focused on a scientific camera. Calcium-independent isosbestic signals were simultaneously captured by alternating excitation with 415 nm LED to dissociate motion, tissue auto-fluorescence, and photobleaching from true changes in fluorescence. All wavelengths were interleaved and collected simultaneously using Bonsai software (Lopes et al., 2015). The sampling rate for the signals was 28 Hz (28 frames per second). Time series were analyzed using an in-house pipeline, and fluorescence signals were normalized to the median for comparison of event amplitude (peak height; % DF/F), frequency (Hz), total fluorescence [area under the curve (AUC)] and duration [full-width half-maximum (FWHM)]. Statistical analyses were performed using Python, and data are reported as mean \pm SEM.

Behavioral testing

Fear conditioning, recall, extinction experiments. On day 1, mice were placed into the shock context A (Cxt A) where they underwent a 360 s contextual fear conditioning session. Foot shocks (1.5 mA, 2 s duration) were administered at the 120, 180, 240 and 300 s time points at 1.5 mA intensity. On day 2, mice were placed back in Cxt A for 360 s of recall where they received shocks on the previous day. There were no shocks administered during this session. On days 3–5, mice were placed back in Cxt A for 900 s without shock administration to extinguish the fear memory across days. At the completion of extinction testing, mice in the no-shock group were administered a single 1.5 mA foot shock to confirm the presence of calcium signal. On day 6, mice underwent a 360 s session of exploration in a novel open field context B (Cxt B) to assess the context-dependent nature of astrocytic calcium changes, if present.

Days 1–5 took place in mouse conditioning chambers (18.5 \times 18.5 \times 21.5 cm; Coulbourn Instruments) with metal-panel side walls, Plexiglas front and rear walls, and a stainless steel grid floor composed of 16 grid bars that were connected to a precision animal shocker that delivered the four foot shocks. A video camera was mounted on a tripod in a front-facing orientation to the conditioning chamber for fear conditioning, recall, and extinction. Day 6 took place in an open field arena (61 \times 61 cm) with black plastic walls and a taped area (45 \times 45 cm) in the middle delineating a center region. For this session, a top-down camera was used to record behavioral video during the session. The chambers were

cleaned with 70% ethanol solution before each animal placement. All behavioral testing was performed during the light cycle of the animal.

Neuronal engram behavioral experiments. Mice were separated into two groups, hM4Di (experimental) and mCherry (control). On day 1, mice were taken off of their Dox diet for 48 h to open the tagging window. On day 3, mice were placed in the same CFC chamber described above, where they received four, 1.5mA foot shocks were administered at 120, 180, 240 and 300s time points during a 360s session. All mice were placed immediately back on Dox after this session. On day 4, mice were placed back in the same conditioned context for a 360 s session of recall. Both groups of mice received a single intraperitoneal injection (3 mg/kg) of clozapine-N-oxide (CNO) 30 min before the session to inhibit the tagged fearful experience. Ninety minutes after the start of recall, mice were transcardially perfused to capture peak cFos protein levels in the BLA because of inhibition of the tagged neuronal ensemble. Mice had calcium dynamics recorded across all three sessions using fiber photometry. For these sessions, a front-facing video camera was used to obtain behavioral videos during fear conditioning and recall, and a top-down-facing video camera was used to obtain home cage video.

Chemogenetic parameters. For chemogenetic silencing of bilateral BLA fear engram neurons, we used the inhibitory designer receptor exclusively activated by designer drugs (DREADDs) hM4Di. hM4Di drives inhibition of infected neurons when bound to the ligand, CNO (Sigma-Aldrich). A 0.6 mg/ml solution of CNO was prepared in sterile saline and 0.5% dimethyl sulfoxide. All mice were intraperitoneally injected with sterile saline for 5 d before experimentation for habituation. On the day of contextual recall, mice were injected with a 3 mg/kg dose of CNO solution 30 min before the start of the session to capture peak drug concentration.

Immunohistochemistry

On day 6, mice were overdosed with 3% isoflurane and perfused transcardially with cold (4°C) PBS followed by 4% paraformaldehyde (PFA; pH, 7.4) in PBS. Brains were extracted and kept in PFA at 4°C for 24–48 h and transferred to a 30% sucrose in PBS solution. Brains were sectioned into 50- μ m-thick coronal sections with a vibratome and collected in cold PBS or 0.01% sodium azide in PBS for long-term storage. Sections were washed three times for 10–15 min with PBS to remove 0.01% sodium azide used for storage. Vibratome sections were incubated for 2 h in PBS combined with 0.2% Triton X-100 (PBST) and 5% bovine serum albumin (BSA) on a shaker at room temperature. Sections were incubated in the primary antibodies mouse monoclonal anti-GFAP (1:1000; NeuroMab), rabbit polyclonal anti-Iba1 (1:1000; Wako Chemicals), and guinea pig anti-NeuN (1:500; Synaptic Systems) diluted in PBST/1% BSA at 4°C for 24 or 48 h. The slices were washed three times for 10–15 min each in 1× PBS. The secondary antibodies were diluted in secondary antibody solution (PBST/1% BSA) and incubated for 2 h at room temperature. The following secondary antibodies were used: Alexa Fluor 555 anti-mouse (1:1000; Invitrogen), Alexa Fluor 555 anti-rabbit (1:1000; Invitrogen), and Alexa Fluor 555 anti-guinea pig (1:200; Invitrogen). The sections were then washed three times with 1× PBS or PBST for 10–15 min each and mounted using VECTASHIELD Mounting Medium with DAPI (Vector Laboratories). Once dry, slides were sealed with clear nail polish on each edge and stored in a slide box in the refrigerator (4°C). Mounted slices were imaged using a confocal microscope (LSM800, Zeiss).

For activity-dependent (engram) experiments, immunohistochemistry was performed as described above with the use of the primary antibodies chicken anti-GFP (1:1000; Invitrogen) and guinea pig anti-RFP (1:1000; Synaptic Systems) and secondary antibodies Alexa Fluor 488 goat anti-chicken (1:200; Invitrogen) and Alexa Fluor 555 goat anti-guinea pig (1:200; Invitrogen) to confirm coexpression of hM4Di-mCherry (RFP) and GfaABC1D-GCaMP6f (GFP) in the BLA. The cFos protein counts across hM4Di and mCherry groups were performed using the additional primary antibody rabbit polyclonal anti-cFos (1:1000; Synaptic Systems) and secondary antibody Alexa Fluor 647 goat anti-rabbit (1:200; Invitrogen).

Brains from all mice used in fiber photometry experiments were analyzed to check adequate fiber location and proper and selective viral

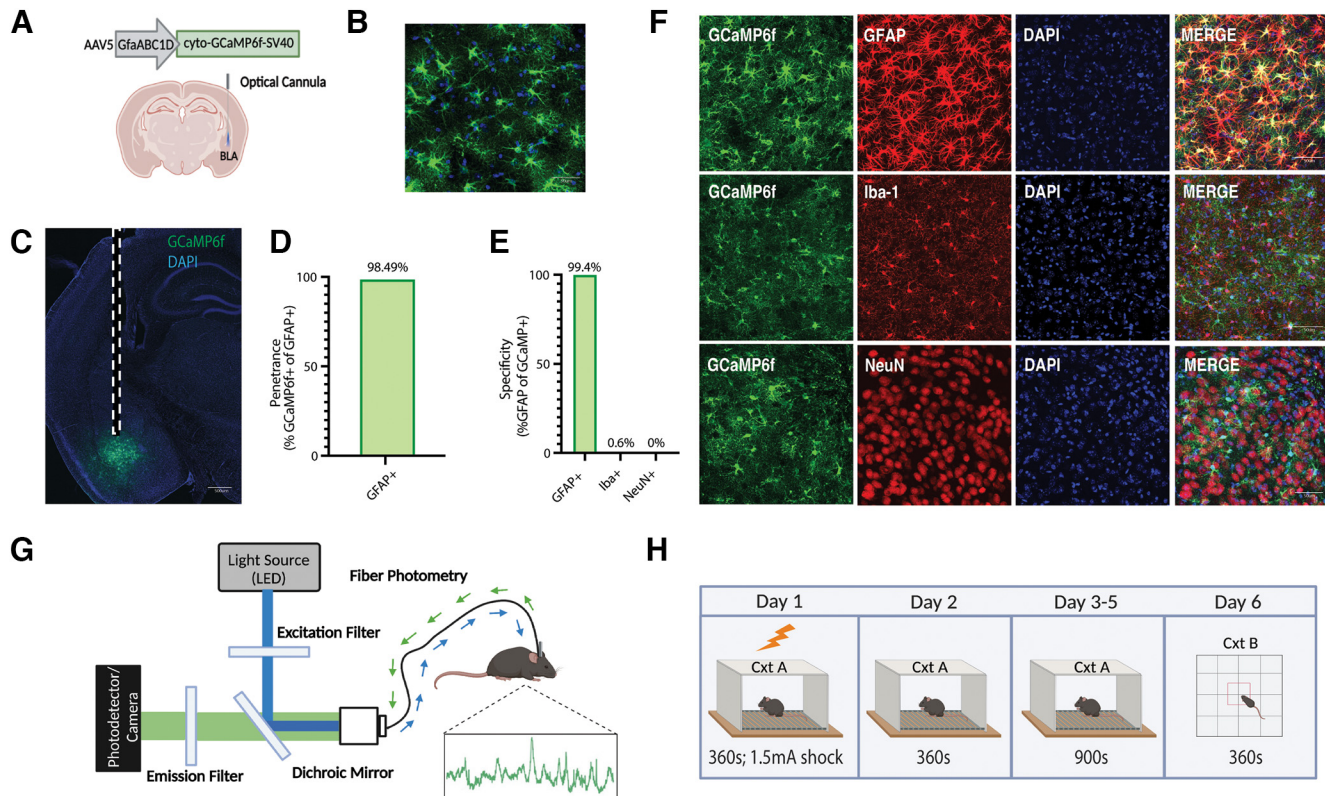


Figure 1. Population-level calcium recordings of basolateral amygdala astrocytes across contextual fear conditioning, recall, and extinction. **A**, Viral strategy and fiber implantation strategy for shock and no-shock conditions. The GECI AAV5-GfaABC1D-cyto-GCaMP6f-SV40 was unilaterally injected into the BLA region of wild-type mice. **B**, **C**, Representative image of GFAP-GCaMP6f+ (green) and DAPI+ (blue) cell expression within the BLA at 20 \times magnification (**B**) and 10 \times magnification (**C**). Scale bar, 500 μ m. Dashed white lines indicate the approximate location of the unilateral fiber implantation. **D**, Penetrance of GCaMP6f (2251 GCaMP6f+/2381 GFAP+ = 98.49%; n = 3; 4 slices/mouse). **E**, Specificity of GCaMP6f (4 Iba-1+/662 GCaMP6f+ = 0.604% microglia; 0 NeuN+/1064 GCaMP6f+ = 0.00% neurons; 2242 GFAP+/2256 GCaMP6f+ = 99.4% astrocyte; n = 3; 4 slices/mouse). **F**, Representative expression of GCaMP6f expression and overlap with microglial (Iba-1), astrocytic (GFAP), and neuronal (NeuN) markers. Scale bar, 50 μ m. **G**, *In vivo* fiber photometry setup. A 470 nm LED delivered an excitation wavelength to GCaMP6f-expressing astrocytes via a patch cord and single fiber optic implant in freely moving mice. The emitted 530 nm signal from the indicator was collected via the same patch cord and fiber, spectrally separated using a dichroic mirror, passed through a series of filters and focused on a scientific camera. A representative calcium time series trace is shown for astrocytic calcium. Calcium-independent isosbestic signal was recorded simultaneously to account for motion, tissue autofluorescence, and photobleaching across time. **H**, Behavioral paradigm; mice underwent CFC on day 1 in Cxt A for 360 s where they received four 1.5 mA foot shocks. On day 2, mice were placed back into Cxt A for contextual recall for 360 s in the absence of foot shock. On days 3–5, mice underwent three contextual extinction sessions for 900 s each. On day 6, mice were placed in Cxt B for 360 s. Mice were perfused and brains extracted for histologic assessment.

expression. Animals that did not meet the criteria for proper fiber location and virus expression were discarded.

Imaging and cell counting

Imaging was performed using a Zeiss LSM 800 epifluorescence microscope with 10 \times and 20 \times objectives using Zen 2.3 software. Full slice images of BLA GfaABC1D-GCaMP6f (green) and DAPI (Fig. 1C) were captured with a 10 \times objective (6554 \times 9319 pixels) along with a zoomed-in (1024 \times 1024 pixels) single-tile z-stack at 20 \times magnification (Fig. 1B).

The cellular specificity and penetrance of the GCaMP6f viral vectors (Fig. 1D–F) was tested by immunohistochemical analysis of the BLA. These images of NeuN, Iba-1, and GFAP were captured in z-stacks of the BLA at 20 \times magnification; 20 \times magnification, single-tile (1024 \times 1024 pixels) representative images are shown in Figure 1B. Cell counts for NeuN, Iba-1, GFAP, and overlaps were performed using ilastik, a machine-learning-based image analysis tool (Berg et al., 2019). Of the 2256 cells expressing GCaMP6f (n = 3 mice; three slices), 2242 were astrocytes (identified by GFAP), resulting in a specificity of 99.4%. Of the 662 cells expressing GCaMP6f (n = 3 mice; three slices), four were microglia (identified by Iba-1), resulting in a specificity of 0.6%. Of the 1064 cells expressing GCaMP6f (n = 3 mice; three slices), 0 were neurons (identified by NeuN), resulting in a specificity of 0%. Finally, of 2381 GFAP+ astrocytes, 2251 were GCaMP6f+ (n = 3 mice; three slices), resulting in a penetrance of 98.49%.

For engram experiments, bilateral BLA was imaged at 20 \times magnification to confirm expression of neuronal hM4Di and mCherry, and single-tile (1024 \times 1024 pixels) images were shown (see Fig. 7B, left). For c-fos counts, bilateral BLA was imaged at 20 \times magnification for n = 3 mice/group times six regions of interest (ROIs) each. In Fiji software (ImageJ), the images were maximum z-projected, each ROI of the BLA was manually isolated and cropped using the polygon tool, and the DAPI and cFos channels were separated for automated counting in ilastik. The cFos+ cells were normalized to the DAPI+ cells for each ROI and averaged across each mouse to generate an average percentage of cFos/DAPI+ (see Fig. 7B, right).

Behavioral analysis

An automated video tracking system, ANY-maze, was used for supervised analysis of freezing bout initiation and termination in the shock context (Cxt A), as well as the total distance traveled, mean speed, number of entries into the center, and total time spent in the center of the open field (Cxt B). Additionally, the pose estimation algorithm, DeepLabCut, was used to perform unbiased animal behavioral evaluation of kinematics (position, acceleration, velocity) for use in generalized linear modeling (GLM; Mathis et al., 2018). These behavioral data were time locked to our fiber photometry time series data for all analyses.

Statistical and fiber photometry analysis

All statistical analysis and subsequent photometry analysis were performed via custom Python scripts freely available at <https://github.com/rsenne/RamiPho>. Our environment was built from the following

software: SciPy (version 1.7.3), statsmodels (version 0.13.2), NumPy (version 1.22.3), Pandas (version 1.4.2), Matplotlib (version 3.5.1), Numba (version 0.55.2), and Seaborn (version 0.11.2).

All photometry signals were baseline corrected using an adaptive iteratively reweighted penalized least-squares method (Zhang et al., 2010). We then performed a simple kernel smoothing to increase the signal-to-noise ratio SNR). For event detection we used a method published previously (Howe et al., 2019). dF/F was calculated by subtracting the median of the trace from the current fluorescence value and then dividing by the median, giving a percentage difference from the median or baseline. We then found any peaks >1 SD away from the mean, in both the positive and negative direction. We then determined the minimum width such that the ratio of positive to total transients (negative and positive) was ≥ 0.99 . Any transients below this width were subsequently discarded.

For perievent analysis, we used a t-confidence interval (tCI) method as proposed previously (Jean-Richard-dit-Bressel et al., 2020). For each window of interest, we calculated a 95, 99, and 99.9% confidence interval (CI). If the CI did not contain the null assumption ($dF/F = \text{median of the event window}$), for a period >0.5 s, we concluded that a significant perievent occurred. This type of method does not allow an exact p value and thus is omitted here.

For GLM we fit a model using a Gaussian family and identity link function. We hypothesized that the calcium activity (dF/F) could be explained by a combination of the isosbestic signal, velocity, and acceleration (up to the third degree); the binary freezing values, the animal identification number, and an interaction effect between the animal and a series of basis spline functions for the 10 s following shock presentation; 5 s following initiation of freezing behavior; and 5 s following the termination of freezing. We chose to fit a singular model as opposed to individual models for each model because we wanted to maximize the number of samples to get better fits for coefficients that should be shared across animals (e.g., the contribution of velocity to the trace) while still including the animal-specific terms to account for individual variability within the SNR of each trace (e.g., the interaction effect between the animals and splines will give unique coefficients for each animal helping to model discrete events better). Thus, our model can be summarized as follows:

$$y_i = \beta_0 + \beta_1 I + \beta_2 F + \sum_j \sum_n \beta_j A n_n + \sum_j \sum_{k=1}^3 \beta_j A^k \\ + \sum_j \sum_{k=1}^3 \beta_j V^k + \sum_j \sum_n \sum_i \beta_j A n_n * P_i + \epsilon,$$

Where I is the isosbestic channel, F is the freezing (binary, 1 is freezing, else 0), $A n$ is a dummy variable encoding animal identification (ID), A is acceleration, V is velocity, P is our polynomial spline functions, k is degree of the polynomial function applied to the kinematic variables, $A n_{tot}$ is the total number of animals, $S p$ is the total number of splines, and β_{fin} is the final index for the specific summation; or more simply stated as follows: $dF/F \sim \text{Isosbestic} + \text{Freezing} + \text{Animal} + \text{Acceleration Functions} + \text{Velocity Functions} + \text{Animal Specific Splines} + \text{Error}$.

The above model is now considered the full model as this is the highest-order model possible for our analysis. To do model selection, simpler models were tested, and when nested, a maximum likelihood ratio test was performed to determine the final model. If comparing two models that were not nested, the Akaike Information Criterion was used.

Data availability

The data that support the findings of this study are available from the corresponding author on reasonable request. All statistical analysis and subsequent photometry analysis was performed via custom Python scripts freely available at <https://github.com/rsenne/RamiPho>.

Results

Astrocytes in the basolateral amygdala are actively involved in fear memory (Stehberg et al., 2012; Liao et al., 2017; Fan et al.,

2021; Shelkar et al., 2021; Lei et al., 2022), but their real-time dynamics during the acquisition and maintenance of conditioned fear in mice is relatively unknown. We monitored astrocyte calcium levels in the BLA using fiber photometry in freely behaving mice across the acquisition, retrieval, and extinction of conditioned fear. Wild-type mice were injected unilaterally with AAV-GfaABC1D-cyto-GCaMP6f to express the GECI GCaMP6f selectively in astrocytes (Fig. 1A–C). To quantify the penetrance and specificity of our viral system, we colabeled GCaMP6f+ cells with GFAP, Iba-1, and NeuN, markers for astrocytes, microglia, and neurons, respectively (Fig. 1D,F). Of 2381 GFAP+ cells, 2251 were GCaMP6f+ ($n = 3$; four slices/mouse), resulting in a penetrance of 98.49% (Fig. 1D,F). Of 662 GCaMP6f+ cells, 4 were Iba1+, resulting in a specificity of 0.604% for microglia (Fig. 1E,F). Of 1064 GCaMP+ cells, 0 were NeuN+, resulting in a specificity of 0.0% for neurons (Fig. 1E,F). Finally, of 2256 GCaMP+ cells, 2242 were GFAP+, resulting in a specificity of 99.4% for astrocytes (Fig. 1E,F).

To test the hypothesis that astrocytes play an active role in the acquisition and maintenance of contextual fear, we used *in vivo* fiber photometry to record their activity across all experimental days of our behavioral task (Fig. 1G,H). Recent literature using calcium imaging in ventral hippocampus (vHPC) has shown that a subset of BLA-vHPC projecting neurons were responsive to aversive shock during CFC (Jimenez et al., 2020). This provides ample evidence that BLA neurons and astrocytes are also likely to be shock responsive. On day 1, mice underwent contextual fear conditioning with the administration of 1.5 mA foot shocks at 120, 180, 240, and 300 s time points (Fig. 1H). To assess whether BLA astrocytes responded specifically to foot shock, we performed perievent analysis to determine whether calcium transients were temporally locked to foot shock. We used a tCI method to classify significant perievents around a time point of interest as previously described (Jean-Richard-dit-Bressel et al., 2020; see above, Materials and Methods). Astrocytes in the shock group displayed robust increases in population-level calcium at the onset of each foot shock during the session compared with the no-shock condition as shown by a representative calcium time series (percentage dF/F) from each group (Fig. 2A) and raster plots (z -scored percentage dF/F) including all mice from each group (Fig. 2D,E). Further analysis revealed that the shock group had significantly increased the percentage dF/F from baseline after the onset of each foot shock compared with the no-shock condition (foot shock perievent analysis; 99% CI; Fig. 2B). Specifically, the shock group had an increase of 44.6% dF/F from baseline after the onset of each foot shock, on average, compared with a 1.6% increase dF/F for the no-shock condition (independent samples t test, Welch's correction, $p = 0.0022$; Fig. 2C).

We next tested the hypothesis that astrocytes modulate their behavior in response to the initiation and/or termination of freezing. There were significant perievents, where the event started before the initiation of freezing (freeze initiation perievent analysis; 99% CI; Fig. 2F) and the termination of freezing (freeze termination perievent analysis; 99% CI), which indicates that astrocytic signaling becomes coupled to freezing behavior during fear memory acquisition (Fig. 2G). Behaviorally, mice in the shock group had a higher freezing across the 360 s session, compared with the no-shock group that did not experience a foot shock (independent t test, $p < 0.0001$; Fig. 2H). The shock group successfully acquired fear across the CFC session compared with the no-shock condition [two-way ANOVA with repeated measures (RM); interaction, $F_{(5,80)} = 10.14$, $p < 0.0001$; time bin, $F_{(1,750,28,00)} = 13.02$, $p = 0.0002$; group, $F_{(1,16)} = 23.59$, $p = 0.0002$; subject,

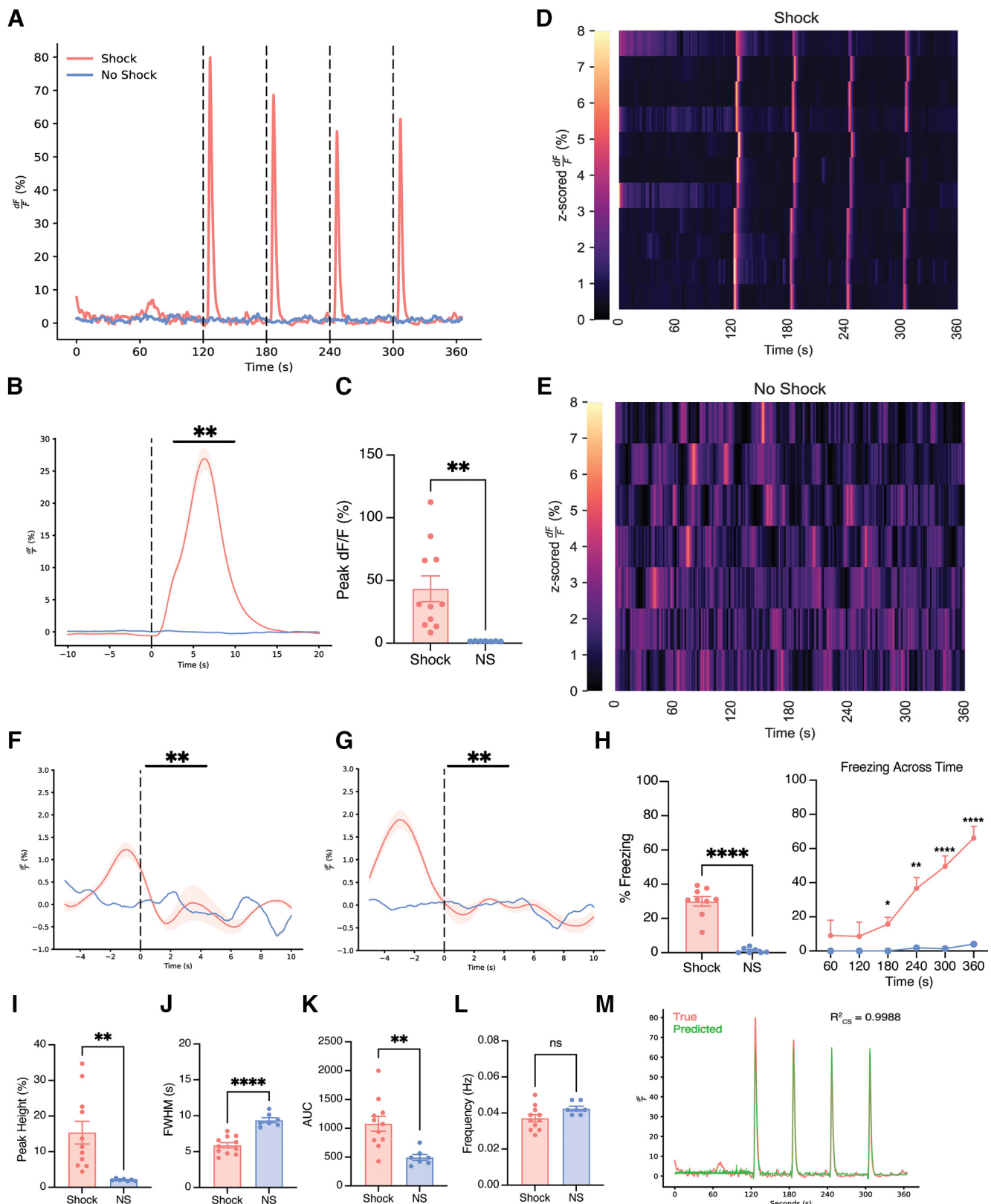


Figure 2. Basolateral amygdala astrocytes robustly respond to foot shock during contextual fear conditioning and exhibit unique calcium event dynamics compared with no-shock controls. **A**, Representative calcium time series (dF/F percentage) for shock and no-shock conditions during the 360 s CFC session; 1.5 mA foot shocks occurred at the 120, 180, 240 and 300 s time points, as indicated by vertical dashed lines. **B**, Perievent analysis for 1.5 mA foot shock, with the onset of foot shock occurring at the dashed line (time = 0). **C**, Quantification of the average percentage change in peak dF/F at the onset of foot shock. **D, E**, The z-scored dF/F (percentage) across CFC for shock (**D**) and no-shock conditions (**E**); each row represents a single subject across time within the session. **F, G**, Perievent analysis for the initiation (**F**) and termination (**G**) of freezing behavior, with each event occurring at the dashed line (time = 0). **H**, Average percentage freezing (left) and freezing across time within the CFC session (right). **I–L**, Calcium event metrics: peak height (**I**), full-width half-maximum (**J**), area under the curve (**K**), and frequency (**L**). **M**, True (pink) and predicted (green) produced from a generalized linear model. All error bars and bands indicate standard error of the mean (SEM). For t tests and ANOVAs, $p \leq 0.05$, ** $p \leq 0.01$, *** $p \leq 0.001$, **** $p \leq 0.0001$; ns, Not significant. For

$F_{(16,80)} = 4.593$, $p < 0.0001$; Fig. 2H). Post hoc analysis demonstrated significant group differences in freezing at the 180, 240, 300, and 360 s time bins (Sidak's multiple comparisons, 180 s, $p = 0.0167$; 240 s, $p = 0.0015$; 300 s, $p < 0.0001$; 360 s, $p < 0.0001$; Fig. 2H).

We calculated event metrics such as peak height, FWHM, AUC, and frequency (events/minute) for shock and no-shock groups. The shock group had significantly increased event peak height, increased AUC, and decreased FWHM compared with no shock during CFC (peak height, independent t test, Welch's correction, $p = 0.0019$; AUC, independent t test, Welch's correction, $p = 0.0011$; FWHM, independent t test, $p < 0.0001$; frequency, independent t test, $p = 0.069$, n.s.; Fig. 2I–L). To further supplement these analyses, we tested whether the astrocytic calcium signals could be decoded as a linear combination of the isobestic channel, freezing, ID number, kinematics, and a set of polynomial spline functions to model the shock response and the initiation and termination of freezing bouts. For a full elaboration of the model and model selection, see above, Materials and Methods, Statistical and fiber photometry analysis. We found that during fear conditioning, the most parsimonious model that could explain the most variability in the dataset contained only the animal-specific splines and kinematic information up to the third degree, meaning that these signals almost entirely encode the shock information and some amount of motion related output. ($R^2_{CS} = 0.9988$; Fig. 2M). Together, the calcium events for the shock condition (i.e., higher amplitude, higher total fluorescence, shorter duration events) suggest that astrocytes become more active after the presentation of a salient stimulus as suggested by the previous literature demonstrating that these cells in dCA1 are responding in a stimulus-dependent manner (Adamsky et al., 2018).

Previous studies have shown that manipulation of astrocytes during retrieval of a conditioned fear memory does not affect recent or remote memory recall, although their activity within a given session remained unmeasured (Adamsky et al., 2018; Kol et al., 2020). To that end, we investigated the real-time dynamics of these cells in mice that received foot shock versus neutral exposure to the same context. On day 2 of our experiment, mice underwent contextual recall without the presence of the unconditioned stimulus (US; foot shock; Fig. 1H). When comparing population-level calcium activity across the shock and no-shock groups, we observed stark differences in the engagement of astrocytes (Figure 3A,B,D). Specifically, we observed that the presence of the US (i.e., foot shock) during fear conditioning continued to engage astrocytes when placed back in the original context, whereas the no-shock group displayed low levels of calcium activity. As the US is the most salient manipulated variable between these two groups, we speculate that astrocytes may be engaged in a learning-dependent manner within the BLA. We also tested the hypothesis that astrocytes modulate their behavior in response to the initiation and/or termination of freezing. There were significant perievents, where the event started before the initiation of freezing (freeze initiation perievent analysis, 99% CI; Fig. 3C) and immediately after the initiation of freezing (freeze termination perievent analysis, 99% CI; Fig. 3E). Behaviorally, mice in the shock group exhibited increased freezing compared with the

no-shock condition that did not receive the conditioned stimulus (CS)/US pairing (Mann–Whitney U test, $p < 0.0001$; Fig. 3F). Across the recall session, mice in the shock group maintained higher levels of freezing compared with no-shock controls (two-way ANOVA RM; interaction, $F_{(5,80)} = 1.163$, $p = 0.3346$; time bin, $F_{(5,80)} = 1.906$, $p = 0.1024$; group, $F_{(1,16)} = 93.18$, $p < 0.0001$; subject, $F_{(16,80)} = 8.924$, $p < 0.0001$; Fig. 3G). Post hoc analysis across groups supported significantly higher levels of freezing in the shock condition during recall across all time bins (Sidak's multiple comparisons; 60 s, $p < 0.0001$; 120 s, $p < 0.0001$; 180 s, $p < 0.0001$; 240 s, $p < 0.0001$; 300 s, $p < 0.0001$; 360 s, $p < 0.0001$; Fig. 3G). Furthermore, to quantify these differences in the traces across groups, we calculated the same average event metrics mentioned above (i.e., peak height, FWHM, AUC, frequency). The shock group had increased average peak height, decreased FWHM, increased AUC, and there were no differences in frequency of events across the session (peak height, independent t test, Welch's correction, $p = 0.0009$; AUC, independent t test, Welch's correction, $p = 0.0156$; FWHM, independent t test, Welch's correction, $p = 0.0005$; frequency, independent t test, Welch's correction, $p = 0.3642$; Fig. 3H–K). This suggests that after context–shock association, astrocytes retain similar calcium dynamics on the following day when placed back in the conditioned environment in the absence of shock. We then fit a Gaussian GLM, as previously described, to determine which variables best accounted for our calcium signal. Interestingly we saw that the kinematic information, freezing, freezing initiation and termination splines, and animal information best accounted for the recall data ($R^2_{CS} = 0.3059$; Fig. 3L). This indicates that during recall there does not seem to be any temporal encoding of the shock that we can detect with this analysis and further suggests that the activity of these astrocytes is tethered to freezing bouts.

To further evaluate the experience-dependent role of astrocytic calcium across the extinction of contextual fear, mice underwent 3 d of extinction on days 3–5 of our behavioral paradigm (Fig. 1H). When comparing astrocytic calcium levels during extinction, we observed higher population activity in the shock group in the absence of the original US compared with the no-shock condition across all 3 d (Fig. 4A–I). This suggests that astrocytes are continuing to be engaged in the shock group and perhaps in a memory-dependent manner as an extinction memory is being formed across days. The no-shock group displayed minimal calcium activity, which may be because of continued exploration of a novel environment as it becomes familiar (Qin et al., 2020). Furthermore, to quantify these differences across groups, we calculated event metrics for each extinction session. For extinction day 1 (EXT1), the shock condition had calcium events with increased peak height, increased AUC, decreased FWHM (i.e., duration of event), and decreased frequency (peak height, independent t test, Welch's correction, $p = 0.0016$; AUC, independent t test, Welch's correction, $p = 0.0036$; FWHM, Mann–Whitney U test, $p = 0.0019$; frequency, independent t test, $p = 0.0253$; Fig. 4J–M). For extinction day 2 (EXT2), the shock condition had calcium events with increased peak height, increased AUC, decreased FWHM, and no difference in frequency (peak height, independent t test, $p = 0.0001$; AUC, independent t test, $p < 0.0001$; FWHM, Mann–Whitney U test, $p = 0.0043$; frequency, independent t test, $p = 0.2050$; Fig. 4J–M). Finally, for extinction day 3 (EXT3), the shock condition had calcium events with increased peak height but no significant differences in FWHM, AUC, or frequency compared with no-shock controls (peak height, independent t test, $p = 0.0010$; AUC, independent t test, Welch's correction, $p = 0.126$; FWHM,

←

perievent metrics, *95% CI, **99% CI; ns. For t tests and ANOVAs, shock $n = 11$, no shock $n = 7$. For foot shock perievents, shock $n = 11$, no shock $n = 7$. For freezing perievents, shock $n = 11$, no shock $n = 2$ because of mice not freezing during this session.

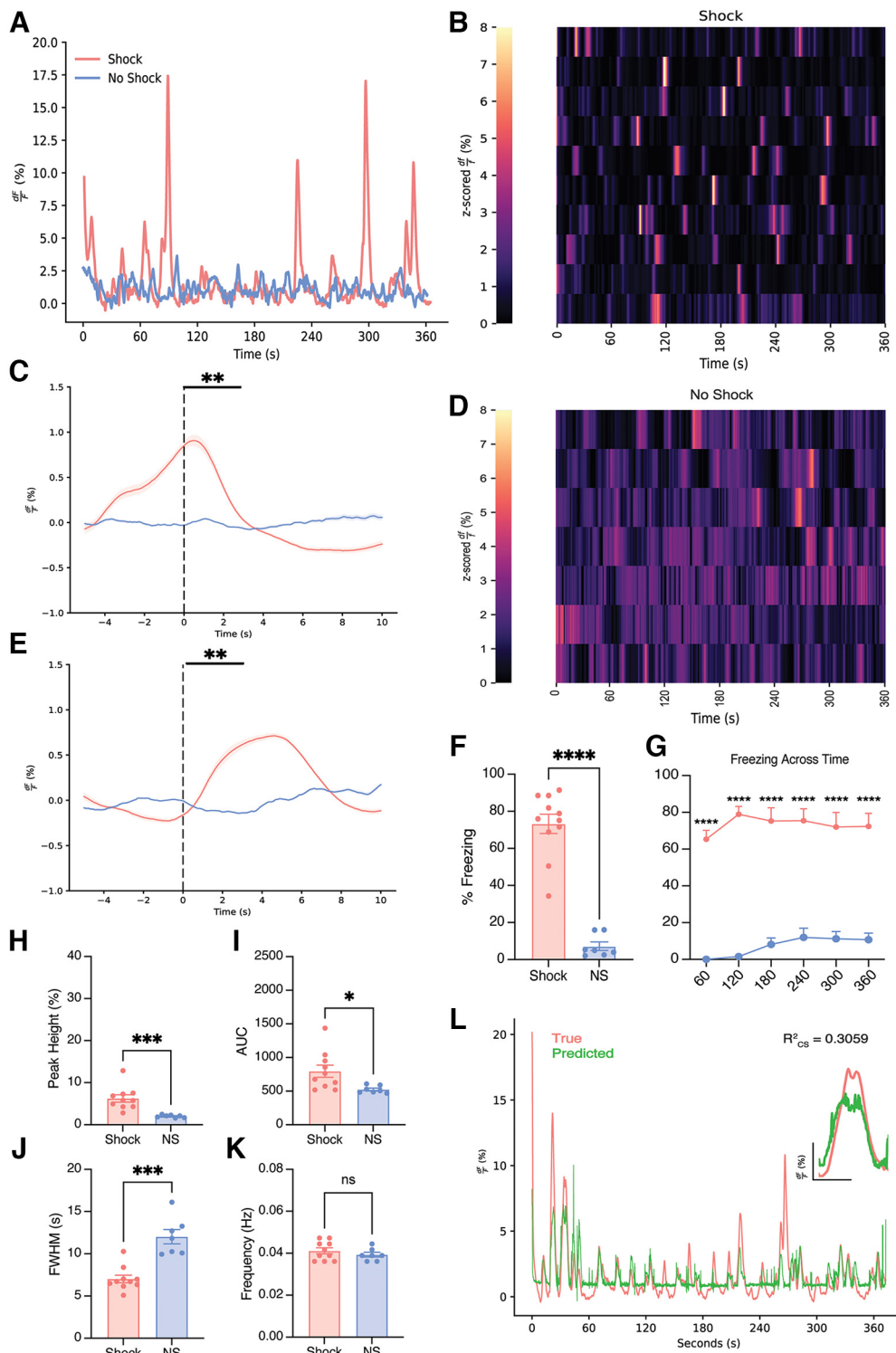


Figure 3. BLA astrocytes respond reliably to the initiation and termination of freezing behavior during contextual recall. **A**, Representative calcium time series (dF/F percentage) for shock and no-shock conditions during the 360 s recall session in the absence of foot shock. **B–E**, The z-scored dF/F (percentage) across recall for (**B**) shock and (**D**) no-shock conditions; each row represents a single subject across time within the session. Perievent analysis for the initiation (**C**) and termination (**E**) of freezing behavior, with each event occurring at the dashed line (time = 0). **F, G**, Behavioral analysis; average percentage freezing (**F**) and freezing across time within the recall session (**G**). **H–K**, Calcium event metrics; peak height (**H**), area under the curve (**I**), full-width half-maximum (**J**), and frequency (**K**). **L**, True and predicted traces produced from a generalized linear model. Error bars indicate SEM. For t tests and ANOVAs, $p \leq 0.05$, ** $p \leq 0.01$, *** $p \leq 0.001$, **** $p \leq 0.0001$; ns, Not significant. For perievent metrics, *95% CI, **99% CI; ns. For t tests and ANOVAs, shock $n = 11$, no shock $n = 7$. For freezing perievents, shock $n = 11$, no shock $n = 6$ because of a mouse not freezing during the recall session.

independent t test, $p = 0.1447$; frequency, independent t test, $p = 0.3851$; Fig. 4J–M). Interestingly, this suggests that astrocytes are initially affected by the presence of the foot shock during CFC but do not adapt further across extinction days. To further

investigate astrocytic calcium responses to freezing behaviors, perievent metrics for the initiation and termination of freezing were calculated as previously performed in contextual recall. Interestingly, astrocytic calcium in the shock group was not

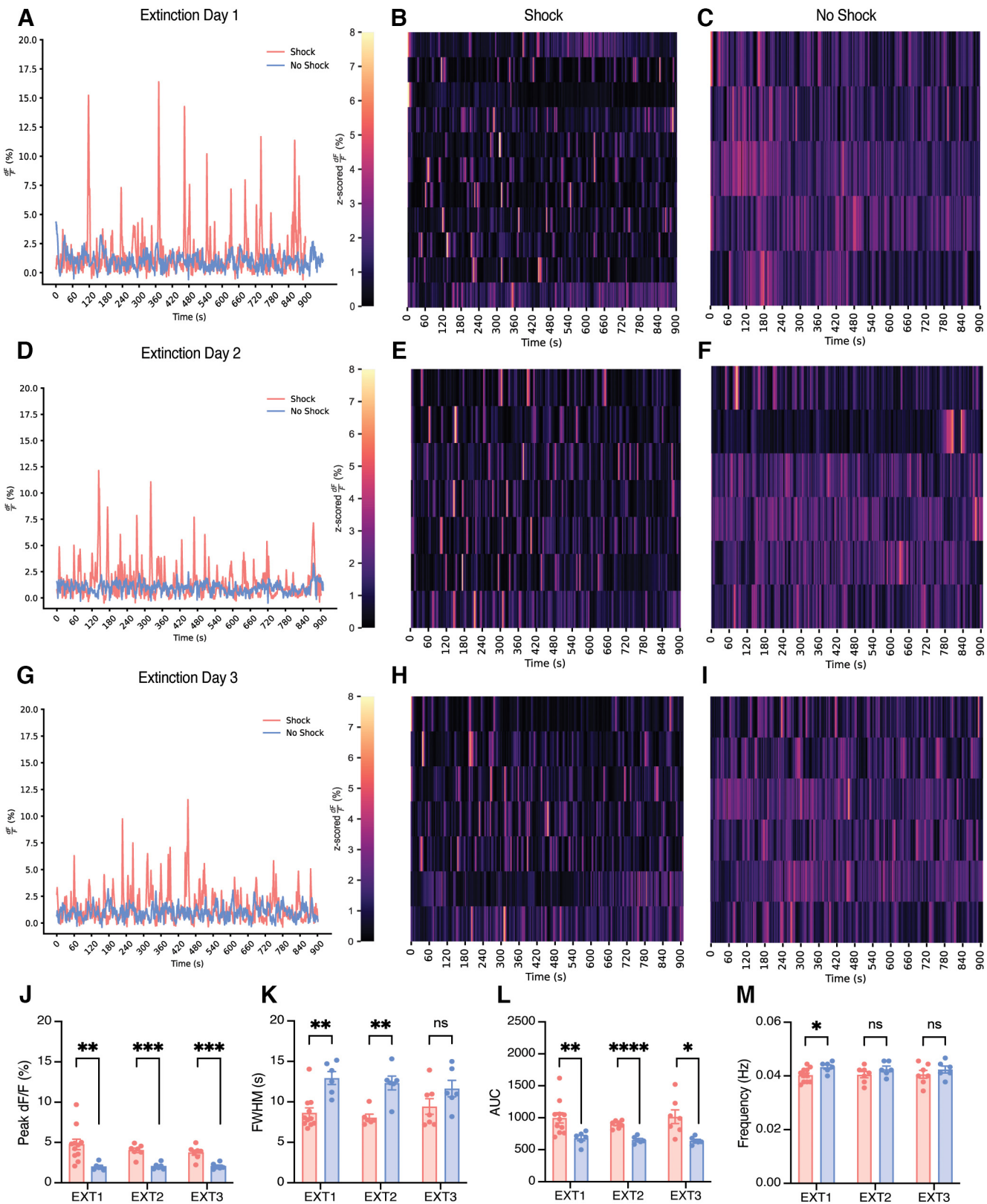


Figure 4. BLA astrocytes in the shock condition exhibit increased peak height, decreased duration, and increased total fluorescence of events compared with no shock, but these do not change across extinction days. **A–I.** Representative calcium time series (dF/F percentage) for shock and no-shock conditions during the 900 s contextual extinction sessions; extinction day 1 (EXT1) (A), extinction day 2 (EXT2) (D), extinction day 3 (EXT3) (G). **B, E, H.** The z-scored dF/F (percentage) across extinction for shock condition; each row represents a single subject across time within the session. **C, F, I.** The z-scored dF/F (percentage) across extinction for the no-shock condition; each row represents a single subject across time within the session. **J–M.** Calcium event metrics; peak height (J), full-width half-maximum (K), area under the curve (L), and frequency across all three d of extinction (M). Error bars indicate SEM. For *t* tests, $p \leq 0.05$, ** $p \leq 0.01$, *** $p \leq 0.001$, **** $p \leq 0.0001$; ns, Not significant. Extinction 1, shock $n = 11$, no shock $n = 6$ (For the no-shock group, recording for one animal was ~ 90 s short. This animal was excluded from the raster plot and behavioral analysis but still used for event metric calculations). Extinction 2, shock $n = 7$, no shock $n = 6$. Extinction 3, shock $n = 7$, no shock $n = 6$.

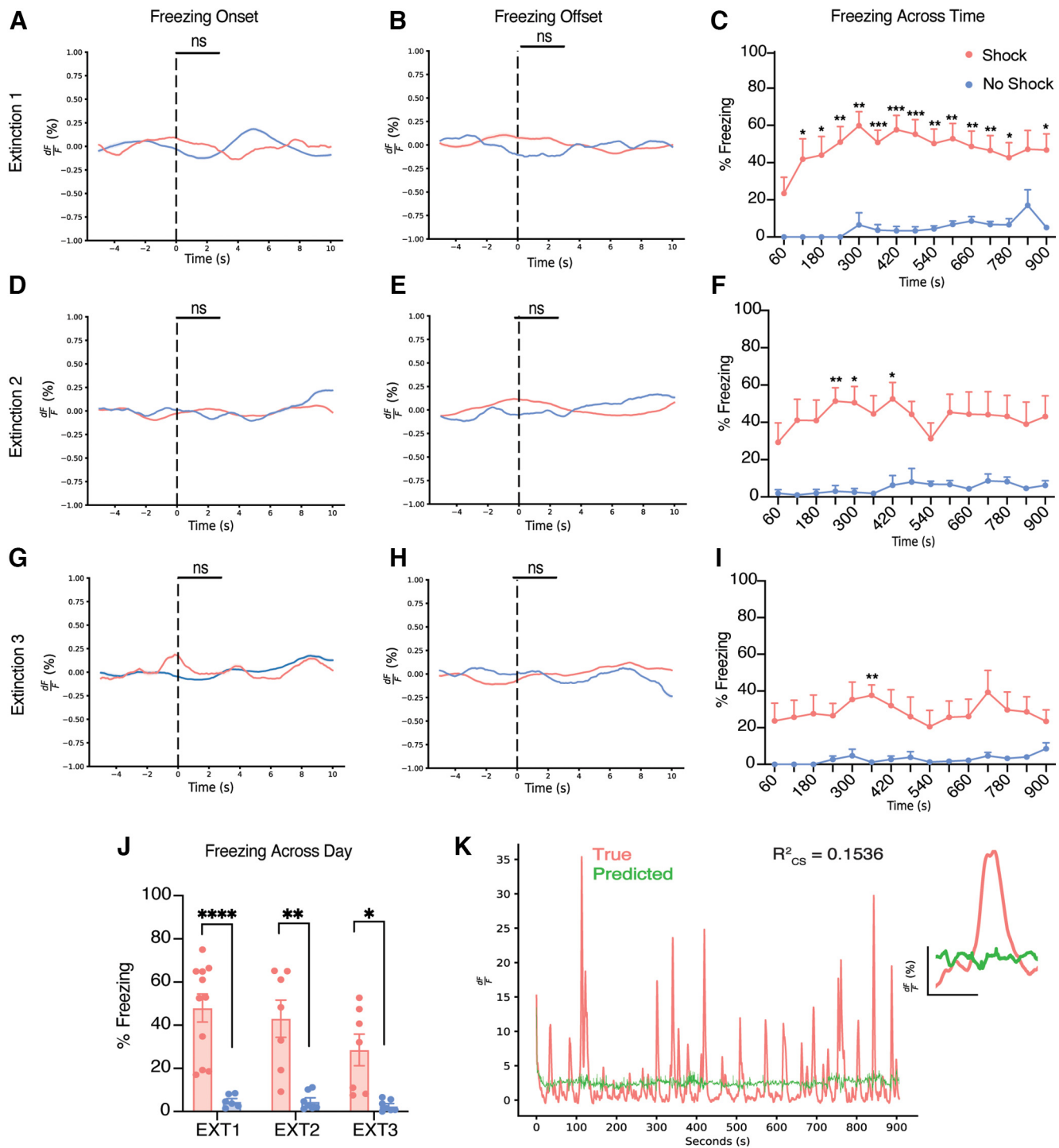


Figure 5. BLA astrocytic calcium does not respond to the initiation or termination of freezing behavior during extinction sessions. **A–I**, Perievent analysis for the initiation (**A**) and termination (**B**) of freezing behavior, with each event occurring at the dashed line (time = 0) for extinction day 1. Perievent analysis for the initiation (**D**) and termination (**E**) of freezing behavior, with each event occurring at the dashed line (time = 0) for extinction day 2. Perievent analysis for the initiation (**G**) and termination (**H**) of freezing behavior, with each event occurring at the dashed line (time = 0) for extinction day 3. Percentage freezing across time within extinction day 1 (**C**), extinction day 2 (**F**), and extinction day 3 (**I**). **J**, Average percentage freezing across 3 d of extinction for shock and no-shock conditions. **K**, True and predicted traces produced from a generalized linear model. Error bars indicate SEM. For *t* tests and ANOVAs, $p \leq 0.05$, $**p \leq 0.01$, $***p \leq 0.001$, $****p \leq 0.0001$; ns, Not significant. For perievent metrics, $^*95\% \text{ CI}$, $^{**}99\% \text{ CI}$; $^{***}99.9\%$; ns. Extinction 1, shock $n = 11$, no shock $n = 6$. (For the no-shock group, the recording for one animal was ~ 90 s short. This animal was excluded from the raster plot and behavioral analysis but still used for event metric calculations). Extinction 2, shock $n = 7$, no shock $n = 6$. Extinction 3, shock $n = 7$, no shock $n = 6$.

responsive to the initiation or termination of freezing behavior for all extinction sessions (freeze initiation and termination perievent analysis; ns; Fig. 5A,B,D,E,G,H). Behaviorally, mice in the shock group exhibited higher average levels of freezing than the no-shock condition group for all 3 d

(extinction 1, independent *t* test, Welch's correction, $p < 0.0001$; extinction 2, independent *t* test, Welch's correction, $p = 0.0042$; extinction 3, independent *t* test, Welch's correction, $p = 0.0123$; Fig. 5J). For each extinction session, shocked mice displayed higher levels of freezing at each time bin than no-

shock controls (extinction 1, two-way ANOVA RM, interaction, $F_{(14,210)} = 1.140$, $p = 0.3247$; time bin, $F_{(4,530,67.95)} = 1.726$, $p = 0.1467$; group, $F_{(1,15)} = 22.92$, $p = 0.0002$; subject, $F_{(15,210)} = 18.83$, $p < 0.0001$); extinction 2, two-way ANOVA RM, interaction, $F_{(14,168)} = 1.204$, $p = 0.2765$; time bin, $F_{(4,306,51.68)} = 1.364$, $p = 0.2574$; group, $F_{(1,12)} = 18.86$, $p = 0.0010$; subject, $F_{(12,168)} = 30.92$, $p < 0.0001$; extinction 3, interaction, $F_{(14,168)} = 0.9191$, $p = 0.5395$; time bin, $F_{(3,186,38.23)} = 1.160$, $p = 0.3392$; group, $F_{(1,12)} = 12.14$, $p = 0.0045$; subject, $F_{(12,168)} = 25.16$, $p < 0.0001$; Fig. 5C,F,I). Specifically, *post hoc* analysis for extinction days revealed specific time bin differences across groups, and this declines across extinction days (extinction 1, Sidak's multiple comparisons, 120 s, $p = 0.0470$; 180 s, $p = 0.0202$; 240 s, $p = 0.0016$; 300 s, $p = 0.0013$; 360 s, $p = 0.0002$; 420 s, $p = 0.0003$; 480 s, $p = 0.0007$; 540 s, $p = 0.0020$; 600 s, $p = 0.0028$; 660 s, $p = 0.0094$; 720 s, $p = 0.0073$; 780 s, $p = 0.0155$; 900 s, $p = 0.0105$; extinction 2, Sidak's multiple comparisons, 240 s, $p = 0.0039$; 300 s, $p = 0.0187$; 420 s, $p = 0.0181$; extinction 3, Sidak's multiple comparisons, 360 s, $p = 0.0094$; Fig. 5C,F,I). We again fit a GLM to determine whether any variables could partially describe our calcium signals. We found that the best fit model included the isosbestic channel and kinematic information ($R^2_{CS} = 0.1536$; Fig. 5K). Interestingly, freezing initiation and termination splines no longer significantly explained any variance within the model, suggesting the astrocytic signals were becoming decoupled to these moments. Through repeated exposures to the context, although calcium events are still present, the amount of information that is able to be decoded from them decreases, suggesting that these signals are more relevant to internal states. Overall, our data suggest that astrocytic calcium remains elevated even as freezing levels decline naturally across extinction sessions.

To further explore the memory-dependent nature of the observed astrocytic calcium changes, a subset of mice from the shock and no-shock groups was placed into a novel open field context (Cxt B) on day 6 of our behavioral paradigm while recording astrocytic calcium (Figs. 1H, 6A–C). Here, we did not observe any significant differences in distance traveled, mean speed, number of center entries, or total time spent in the center of the open field across shock and no-shock conditions (distance, independent *t* test, $p = 0.2773$; mean speed, independent *t* test, $p = 0.2750$; center entries, independent *t* test, $p = 0.3681$; center time, independent *t* test, $p = 0.42547$; Fig. 6D–G). Further, most mice in both groups did not freeze at all for the entirety of the open field session; thus, we did not further analyze freezing behavior between groups or perform perievent analysis with astrocytic calcium for freezing initiation or termination as performed with other sessions. Most important, we assessed calcium event metrics during this session to observe whether changes observed during contextual fear learning and extinction are because of an enhancement in activity maintained over time. Here, we did not observe any significant differences in the peak height, AUC, FWHM, or frequency of calcium events across the shock and no-shock conditions (peak height, Mann–Whitney *U* test, $p = 0.3429$; FWHM, independent *t* test, $p = 0.7049$; AUC, independent *t* test, $p = 0.6321$; frequency, independent *t* test, $p = 0.3262$; Fig. 6H–K). This suggests that astrocytic calcium activity changes because of shock are context dependent, and these cells are storing information related to the memory of the aversive experience.

To further elucidate the role of astrocytes in context-dependent memory recall, we used the Tet-Tag (tetracycline transactivator controlled genetic tagging of active neural circuits) activity-

dependent labeling strategy to chemogenetically inhibit a fear memory while simultaneously performing astrocytic fiber photometry recordings (Fig. 7A, left). This system relies on the coupling of the *c-fos* promoter to the tetracycline transactivator (tTA), which in its protein form binds directly to the tetracycline response element (TRE) in a Dox-dependent manner and can drive expression of a protein of interest (e.g., hM4Di and/or mCherry; Fig. 7A, left). Moreover, the expression of the DREADD, hM4Di, allows for chemogenetic silencing of the tagged experience (i.e., fear) during recall. To confirm successful perturbation of the hM4Di-expressing engram neurons in bilateral BLA, we killed mice 90 min after the start of the behavioral recall session to capture peak endogenous cFos protein levels. We found that across the groups, there was a significant increase in *c-fos*⁺ cells in the hM4Di compared with the mCherry controls (independent *t* test, $p = 0.0023$; Fig. 7B). This increase in cFos with inhibition of a cellular population in the BLA may seem counterintuitive, but it has become clear in recent studies that modulation of neurons with chemogenetics results in differential effects on *c-fos* and behavior. For example, inhibition of BLA engram cells during chronic hippocampal stimulation resulted in equivalent levels of cFos across the hM4Di and control groups (Chen et al., 2019). We posit that CNO may have induced rebound activity in the neighboring nontagged cells of the BLA through local circuit mechanisms. Additionally, previous work from our lab has shown that chemogenetic inhibition of engram cells in dorsal CA1 of the hippocampus increased cFos in neighboring nonengram cells, which we also believe points to a local circuit rebound of neuronal activity in response to inhibition (Trouche et al., 2016; Grella et al., 2020).

As shown in our experiments above, we began by performing simultaneous astrocytic calcium recordings with fiber photometry through the expression of AAV5-GfaABC1D-cyto-GCaMP6f in the unilateral BLA (Fig. 7A, left). Previous literature has demonstrated that manipulation of the BLA with perturbation techniques has an impact on behavioral freezing levels typically associated with context-dependent recall (Han et al., 2009; Liu et al., 2012; Gore et al., 2015; Liu et al., 2022). We hypothesized that bilateral inhibition of tagged BLA engram neurons expressing hM4Di during recall would disrupt astrocytic calcium dynamics that we observed in our first experiment. On day 1, mice had Dox diet removed to open the tagging window 48 h later. On day 3, mice underwent a 360 s CFC session with the administration of 4, 1.5 mA foot shocks, as described in our previous experiments, while astrocytic calcium dynamics were recorded in BLA (Fig. 7A, right). Immediately after this CFC session, mice were placed back on their Dox diet to ‘close’ the tagging window (Fig. 7A; right). On day 4, mice underwent a 360 s contextual recall session in the absence of foot shocks. Thirty minutes before this session, mice received an intraperitoneal injection of CNO at 3 mg/kg to inhibit the tagged fear neuronal ensemble during behavior (Fig. 7A, right). Expression of hM4Di-mCherry in bilateral BLA with astrocytic GCaMP was confirmed in each animal before behavioral and calcium time series analysis (Fig. 7B).

When comparing astrocytic calcium levels during CFC, both hM4Di and mCherry groups displayed robust increases at the initiation of each foot shock (120 s, 180 s, 240 s, 300 s), as described above (Fig. 7C). This was expected as no CNO was on board during the CFC session, and we anticipated replication of our above findings. Additionally, in both groups there was time locking to behavioral freezing initiation and termination epochs

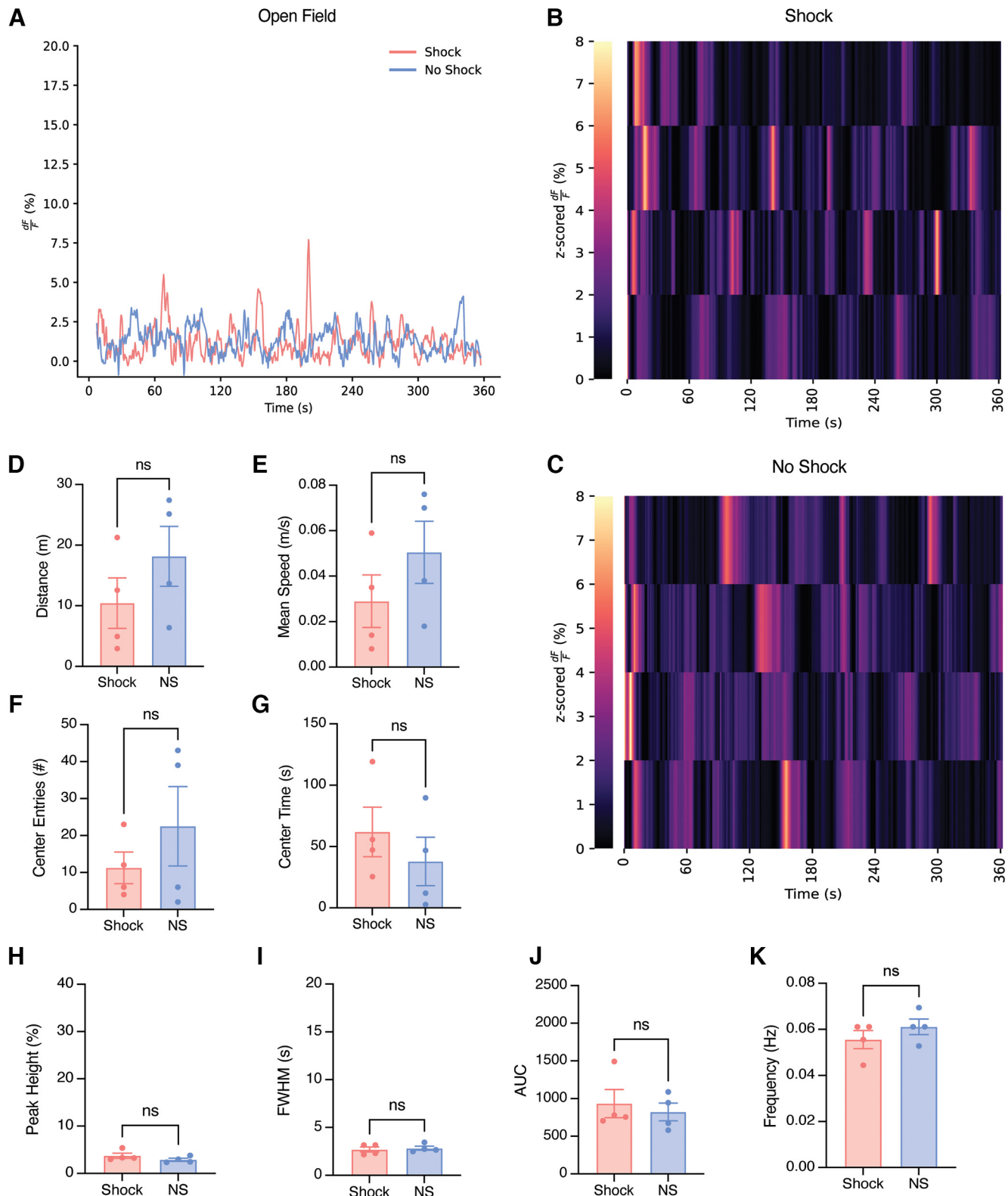


Figure 6. Astrocytic calcium event characteristics and behavior in a novel open field environment do not differ between shock and no-shock groups. **A**, Representative calcium time series ($\Delta F/F$ percentage) for shock (coral) and no-shock (blue) conditions during the 360 s novel open field Cx t B session. **B, C**, The z-scored $\Delta F/F$ (percentage) in Cx t B for shock and no-shock conditions; each row represents a single subject across time within the session. **D–G**, Behavioral measures; distance traveled (m; **D**), mean speed (m/s; **E**), number of center entries (**F**), and time spent in the center (**G**). **H–K**, Calcium event metrics; peak height (%; **H**), full-width half-maximum (s; **I**), AUC (**J**), and frequency (Hz; **K**). Error bars indicate SEM. For *t* tests, $p \leq 0.05$, ** $p \leq 0.01$, *** $p \leq 0.001$, **** $p \leq 0.0001$; ns, Not significant. Open field Cx t B, shock $n = 4$, no shock $n = 4$.

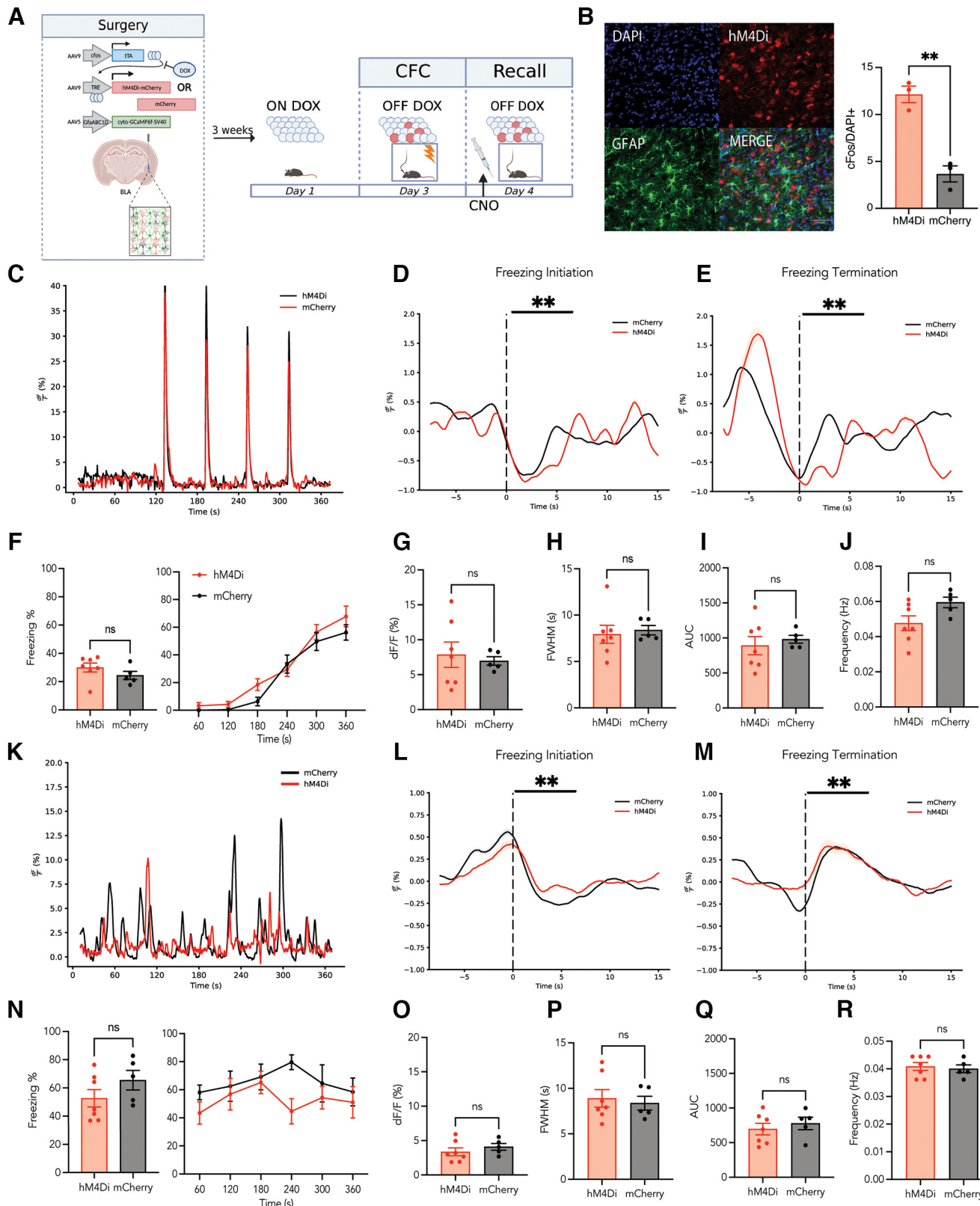


Figure 7. Neuronal fear engram inhibition in the BLA during recall does not modify freezing behavior or astrocytic calcium event characteristics. **A**, Surgical and behavioral schematic. The genetically encoded calcium indicator, AAV5-GfaABC1D-cyto-GCaMP6f-SV40, was unilaterally injected into the BLA in combination with bilateral injection of either AAV9-c-fos-tTA-TRE-hM4Di-mCherry (hM4Di) or AAV9-c-fos-tTA-TRE-mCherry (mCherry) control virus to allow chemogenetic control of labeled cells while recording astrocytic calcium dynamics. On day 1, mice were taken off of their Dox diet to allow for the opening of the labeling window 48 h in advance of behavioral testing. On day 3, mice underwent CFC on day 1 in Cxt A for 360 s where they received four 1.5 mA foot shocks. They were immediately placed back on their Dox diet, thus closing the labeling window. On day 4, mice were placed back into Cxt A for contextual recall for 360 s in the absence of foot shock. Thirty minutes before this session, CNO was administered at 3 mg/kg to inhibit the labeled engram during recall. Ninety minutes after the start of the behavioral session, mice were perfused to capture peak endogenous c-fos protein levels. **B**, Left, Representative images of hM4Di-mCherry/GFAP containing (red and green, respectively) and DAPI+ cells (blue). Right, Bar graph of cFos/DAPI+ cells per field. The hM4Di-mCherry group shows significantly more cFos/DAPI+ cells compared to the mCherry control group (**).

during CFC in both hM4Di and mCherry groups, further replicating our prior experiment (freeze initiation and termination perievent analysis, 99% CI; Fig. 7*D,E*). As expected, hM4Di and mCherry mice displayed the same freezing levels on average (independent *t* test, $p = 0.2395$) and across time during CFC (two-way ANOVA RM, interaction, $F_{(5,50)} = 1.107$, $p = 0.3688$; time bin, $F_{(2,623,26,23)} = 82.43$, $p < 0.0001$; group, $F_{(1,10)} = 1.564$, $p = 0.2395$; subject, $F_{(10,50)} = 3.685$, $p = 0.0010$; Fig. 7*E*). Finally, both groups displayed no significant differences in astrocyte calcium event characteristics (peak height, full-width half maximum, area under the curve, or frequency) during CFC, as expected (peak height, independent *t* test, Welch's correction, $p = 0.6532$; AUC, independent *t* test, Welch's correction, $p = 0.5351$; FWHM, independent *t* test, $p = 0.7292$; frequency, independent *t* test, $p = 0.0623$; Fig. 7*G–J*).

For fear memory recall, mice in the hM4Di and mCherry groups did not display detectable changes in astrocytic calcium dynamics (Fig. 7*K*). This was further confirmed by perievent analysis at the initiation and termination of freezing bouts during recall. As shown in our above experiments, astrocytic calcium becomes time locked to each of these behavioral epochs for both hM4Di and mCherry groups compared with their respective medians (freezing initiation/termination, perievent analysis, 99% CI; Fig. 7*L,M*). This suggests that CNO does not have an effect on astrocytic calcium dynamics during contextual recall. Interestingly, we did not observe any significant differences in behavioral freezing levels between the two groups, suggesting that chemogenetic inhibition of a fear engram in the BLA does not lead to a decrease in freezing levels (independent *t* test, $p = 0.2028$), nor the recall of fear across time within session (mixed-effects model, interaction, $F_{(5,60)} = 0.7030$, $p = 0.6234$; time bin, $F_{(1,60)} = 5.257$, $p = 0.0254$; group, $F_{(5,60)} = 0.6997$, $p = 0.6258$; Fig. 7*N*).

Furthermore, to quantify any differences in astrocytic calcium event metrics, peak height, FWHM, AUC, and frequency (Hz) were analyzed. There were no significant differences in any of these metrics, with both groups mirroring the results described in our initial shock group findings (peak height, independent *t* test, $p = 0.3921$; AUC, independent *t* test, $p = 0.5271$; FWHM, independent *t* test, $p = 0.6981$; frequency, independent *t* test, $p = 0.6860$; Fig. 7*O–R*). Overall, our data suggest that inhibition of a neuronal fear engram in BLA does not have an impact on behavioral freezing levels, nor does it affect astrocytic calcium dynamics. It is important to note, however, that the freezing behavior and its tie to astrocytic calcium was maintained.

←

Scale bar indicates 50 μ m. Right, The percentage of c-fos/DAPI counts in the hM4Di and mCherry groups. *C*, Representative calcium time series (dF/F percentage) for hM4Di (red) and mCherry (black) conditions during the 360 s CFC session. *D, E*, Perievent analysis for the initiation (*D*) and termination (*E*) of freezing behavior during CFC, with each event occurring at the dashed line (time = 0). *F*, Behavioral analysis for CFC. Left, Average percentage freezing. Right, Freezing across time within the recall session. *G–J*, Calcium event metrics for CFC, peak height (*G*), full-width half-maximum (*H*), area under the curve (*I*), and frequency (*J*). *K*, Representative calcium time series (dF/F percentage) for hM4Di (red) and mCherry (black) conditions during the 360 s recall session. *L, M*, Perievent analysis for the initiation (*L*) and termination (*M*) of freezing behavior during recall, with each event occurring at the dashed line (time = 0). *N*, Behavioral analysis for recall. Left, Average percentage freezing. Right, Freezing across time within the recall session. *O–R*, Calcium event metrics for recall, peak height (*O*), full-width half-maximum (*P*), area under the curve (*Q*), and frequency (*R*). All error bars and bands indicate SEM. For *t* tests and ANOVAs, $p \leq 0.05$, ** $p \leq 0.01$, *** $p \leq 0.001$, **** $p \leq 0.0001$; ns, Not significant. For perievent metrics, *95% CI, **99% CI; ns; hM4Di = 7, mCherry = 5.

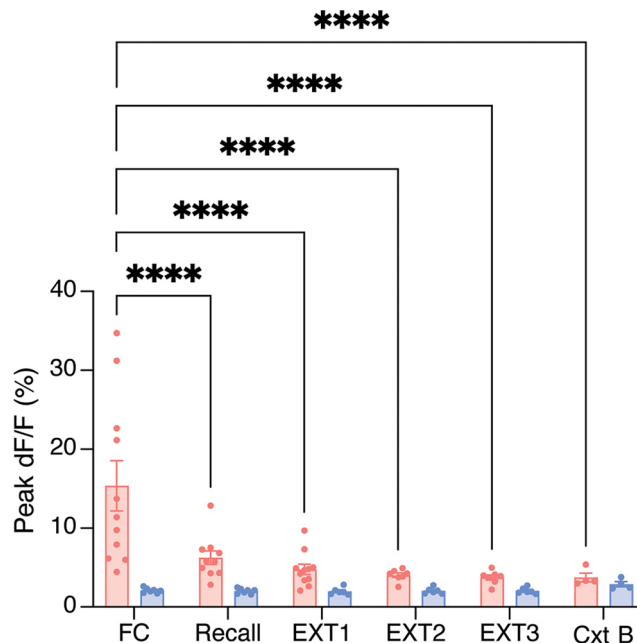


Figure 8. Astrocytic calcium dF/F does not change after contextual fear conditioning. dF/F (percentage) across FC, recall, extinction (EXT1–3), and exposure to the novel open field context (Cxt B). All error bars and bands indicate SEM. For ANOVA, $p \leq 0.05$, ** $p \leq 0.01$, *** $p \leq 0.001$, **** $p \leq 0.0001$; ns, Not significant. Shock $n = 4–11$, no shock $n = 4–7$.

To address the possibility that reduced dF/F (percentage) we see was a function of nonexperience-related effects (i.e., photobleaching caused by repeated recordings), we assessed the peak dF/F (percentage) across days. We found that there were no significant changes in the no-shock group across days, and only the fear conditioning session was significantly different from other days in the shock group (two-way ANOVA, interaction, $F_{(5,74)} = 4.924$, $p = 0.0006$; day, $F_{(5,74)} = 4.769$, $p = 0.0008$; group, $F_{(1,74)} = 19.72$, $p < 0.0001$; Tukey's multiple comparisons, shock, FC vs recall, $p < 0.0001$; FC vs EXT1, $p < 0.0001$; FC vs EXT2, $p < 0.0001$; FC vs EXT3, $p < 0.0001$; FC vs Cxt B, $p < 0.0001$; all other comparisons across days for the shock and no-shock groups were not significant; Fig. 8*A*). This is an unsurprising result as a negative experience like shock could easily cause such robust differences in calcium dynamics that we observed (Fig. 2*A*). From this analysis we can conclude that after fear conditioning the peak dF/F did not change in the shock group, and such alterations in event metrics were not caused by photobleaching or other technical considerations.

Discussion

Our results demonstrate that BLA astrocytes are differentially involved in the acquisition, recall, and extinction of a contextual fear memory. Strikingly, these astrocyte populations in the no-shock groups showed low levels of calcium-dependent activity relative to the shocked group. These results corroborate previous research demonstrating that astrocytic populations are active specifically during salient experiences (Adamsky et al., 2018). Furthermore, this could be related to an increased demand for neuronal metabolic support because of cellular activity recruited during memory formation. Previous models suggest that astrocytes become active during metabolically taxing experiences to support memory encoding and consolidation by providing astrocytically derived lactate to neuronal populations to increase ATP production (Steinman et al., 2016; Adamsky and Goshen, 2018;

Alberini et al., 2018). In line with this possibility, in our study, mice that did not associate a noxious stimulus to the context displayed less activity than the shocked group. This could indicate that during memory acquisition, where a CS is paired with a US, astrocytic populations become involved to maintain this memory association. As the BLA preferentially parses salient information (Sengupta et al., 2018; Pryce, 2018), this could explain the lack of strong calcium events in the no-shock group, whereas in a structure that processes both associations and emotional salience (Eichenbaum et al., 1996; Zheng et al., 2017), such as the hippocampus, we predict to see reliable but increased events during contextual exploration and after CS/US pairing. Relatedly, and given that astrocyte assemblies are remarkably disengaged before the onset of foot shock during CFC in our study, future experiments may test whether populations of astrocytes are necessary for proper fear expression, and if after such salient experiences, BLA neurons require glial participation for stable memory correlates.

Interestingly, we only observed differences in the calcium event characteristics (e.g., FWHM, peak height) in the shock group when animals are undergoing CFC. This could indicate there are two distinct populations of cells, one that becomes active for memory encoding and maintenance, whereas the other is there to process incoming sensory input into the BLA or motor output. This hypothesis is supported by our modeling approach, which reported significant contribution of kinematic related information as well as stimuli specific and relevant behavioral information. Furthermore, although the no-shock animals display minimal calcium transients, these transients are significantly wider, possibly in response to exploring the novel context. This could be explained by the observation that AUC for these transients was also significantly lower for these animals, suggesting there was less overall calcium binding and subsequent recorded fluorescence, and thus indicating there may be cells that had sustained activity in response to a nondiscrete stimuli, in contrast to something well defined like foot shock. Furthermore, perievents were observed in the fear conditioning and recall sessions. Specifically, we observe an increase in activity before the initiation and termination of freezing during recall. During recall, we observe an increase in activity before freezing initiation but instead an increase in activity after the termination of freezing. It is possible that astrocytes ramp up their activity to either induce a state of freezing or become active in response to increased neuronal activation immediately before bouts of freezing. Regarding the termination of a freezing bout specifically, it is possible that astrocytes play a functional role in suppressing fear or anxiety states within the BLA (Cho et al., 2022), although it is important to note that separate studies have also implicated their role in modulating locomotion (Qin et al., 2020); thus, as termination of freezing by definition requires movement, these two explanations remain to be reconciled. Notably, we did not observe these elevations in calcium activity at the initiation or termination of freezing during extinction. Indeed, we lose our predictive power in our GLM during extinction sessions, further evidencing this putative decoupling, and so it is likely these signals reflect internal physiological states that would be interesting to further investigate with higher spatial resolution. This could be because of the difference in session length causing changes to how these cells respond after the initial 6 min, or it could be that after this initial exposure some subsequent learning has occurred causing these cells to respond to different local cues or internal states. Although fiber photometry renders this possibility difficult to test because of its lack of cell-specific granularity, these hypotheses would be interesting to explore with higher resolution *in vivo*

one-photon imaging approaches, which would allow us to visualize multiple subpopulations of BLA astrocytes and could explain the diverse milieu of these signals.

Importantly, our findings that astrocytic calcium dynamics are modulated by salient stimuli were specific to the fear conditioned context, as supported by the lack of astrocytic calcium and behavioral changes in the neutral open field context. This is in line with previous findings showing that astrocytic manipulation enhances memory allocation in a task-specific manner during learning but not in the home cage (Adamsky et al., 2018). Astrocytic activity is heavily dependent on the presence of salient stimuli during a learning experience (i.e., foot shock), and novel exploration of an environment is not sufficient to induce changes in the underlying calcium dynamics of astrocytes. This is congruent with data suggesting that the BLA shows sparse activity that is dependent on salient stimuli (i.e., reward; Pratt and Mizumori, 1998).

Our findings suggest that chemogenetic-mediated neuronal engram inhibition in the BLA during recall does not abolish freezing behavior nor affect astrocytic calcium dynamics. Although other work in the field suggests that BLA engram cells are necessary for fear recall (Han et al., 2009), we speculate that both the behavioral schedules and inhibitory strategies implemented constrain whether a BLA-mediated engram becomes necessary for the behavioral expression of memory. Specifically, previous work directly inhibiting BLA engram cells using the inhibitory opsin ArchT shows a decrease in behavioral freezing during recall, in a light-dependent manner (Zaki et al., 2022). However, this work performed inhibition after the extinction, reinstatement, and recall of this reinstated memory. Thus, the differences in behavioral schedules and phases of learning during which inhibition occurs can influence whether engrams are necessary for the behavioral output of fear during recall. Another technical consideration is that we are using chemogenetics, whereas this previous work used an inhibitory opsin. It is possible that the temporal specificity of the light-driven method was able to more effectively inhibit these engram cells in a behaviorally relevant manner. Additionally, inhibition of a neuronal ensemble overexpressing CREB protein in the BLA resulted in decreased freezing behavior during recall (Han et al., 2009; Rashid et al., 2016). Notably, this finding was in the context of auditory tone conditioning as opposed to contextual fear conditioning in our experiments, which have separate circuits that could explain these differential effects. We believe these differences point to boundary conditions under which BLA-mediated engrams are revealed to be necessary for memory.

Future work may seek to express a pan-neuronal inhibitor throughout the BLA to test whether this global reduction in activity modulates astrocyte dynamics. It is possible that the number of engram cells tagged in the BLA is not sufficient to abolish the behavioral expression of fear, or other brain regions may be compensating for or driving this behavior in coordination with the BLA. Astrocytes may still be intimately associated with engram cells in the BLA, but this perturbation is not sufficient to eliminate their activity. It would be interesting to label BLA engram cells and their associated astrocytes with chemogenetic tools to observe whether the combination of cell inhibition (and thus, expanding the definition of an engram to include glial cells) abolishes memory recall. Promisingly, such strategies that permit labeling and manipulation of both neurons and astrocytes will enable a better understanding of how heterogeneous cell types contribute to the overall memory engram as well as its behavioral expression. Broadly, as we are recording calcium dynamics from

astrocytes in these experiments, it may be possible that neuronal calcium is being modified by hM4Di inhibition, and our approach is unable to capture these changes. However, even if neuronal activity was decreased, astrocytes could be compensating for the behavioral output of fear during recall. A general assumption of this mechanism is that neurons and astrocytes are correlated in their calcium activity (Agulhon et al., 2008; Zhao et al., 2012).

Although our results demonstrate a functional role of astrocytes in fear learning, the BLA is known to process additional salient information including fear, reward, novelty, and so on. For instance, recent studies have shown there are heterogeneous, genetically defined populations within the BLA that may preferentially respond to a variety of stimuli and valences (Kim et al., 2016). Although our experiments did not tease out any valence-specific contributions of astrocytic calcium activity, future studies may deliver multiple valence-specific stimuli (e.g., sweetened condensed milk, social interaction, restraint stress) to animals while recording the corresponding calcium transients in the BLA. We posit that the BLA will display robust calcium dynamics to both positive and negative stimuli, albeit in partially separate populations of cells. This is consistent with previous literature showing there are genetically defined populations of cells along the anterior–posterior axis of the BLA that process fear and reward uniquely (Kim et al., 2016).

Although this work provides a role for astrocytes in conditioned fear, an ongoing issue surrounds whether astrocytes are mere support cells for neurons or if they actively encode information necessary for cognitive processes. Future experiments may concurrently record from neuronal populations to identify putative relationships between each cell type and how real-time interplay between these populations supports learning and memory processes. A tantalizing possibility that combines neuron-glia relationships with neuromodulatory influences is that BLA astrocytes are necessary for proper adrenergic signaling, which has been proposed in prior work (Gao et al., 2016; Akther and Hirase, 2022). Also, it has been shown that CFC induces a down-regulation of astrocytic Rac-1 (Liao et al., 2017; Fan et al., 2021), promoting astrocytic plasticity, which may explain our observed differences in calcium events between our two groups in that this increased astrocytic plasticity could be necessary for remodeling synaptic connections for continued signaling. Further, astrocytes have been shown to contribute to remote memory formation via projection-specific modulation of hippocampal-cortical targets (Kol et al., 2020). It would be interesting to explore astrocytic contributions to the natural forgetting of a fear memory, rather than extinction, on a longer time scale. This could be performed with longitudinal calcium recordings throughout a fear memory paradigm, with the addition of tracking throughout the decrease in freezing behavior that occurs over weeks.

Finally, future studies may causally dissect the role of astrocytes by Gq or Gi pathway activation in these populations during recall or extinction to determine whether cellular manipulation is capable of inducing either a memory-enhancing or amnesic response to fear learning. As astrocytes do not have typical inhibition/excitation properties, which are more typically associated with neurons (Durkee et al., 2019; Van Den Herrewegen et al., 2021), future research may take more complex signaling pathways into account and yield crucial information in how astrocytes participate at the tripartite synapse to facilitate the learning of conditioned fear. Indeed, higher resolution single-cell and populating imaging methods, combined with causal perturbation strategies, could be used to further delineate the role of these cells

in memory formation and expression. Overall, our results suggest an active role of astrocytes in contextual fear learning within the BLA and reveal their dissociable role in contributing to memory recall and extinction.

References

- Adamsky A, Goshen I (2018) Astrocytes in memory function: pioneering findings and future directions. *Neuroscience* 370:14–26.
- Adamsky A, Kol A, Kreisel T, Doron A, Ozeri-Engelhard N, Melcer T, Refaeli R, Horn H, Regev L, Groysman M, London M, Goshen I (2018) Astrocytic activation generates *de novo* neuronal potentiation and memory enhancement. *Cell* 174:59–71.e14.
- Agulhon C, Petracic J, McMullen AB, Sweger EJ, Minton SK, Taves SR, Casper KB, Fiacco TA, McCarthy KD (2008) What is the role of astrocyte calcium in neurophysiology? *Neuron* 59:932–946.
- Akther S, Hirase H (2022) Assessment of astrocytes as a mediator of memory and learning in rodents. *Glia* 70:1484–1505.
- Alberini CM, Cruz E, Descalzi G, Bessières B, Gao V (2018) Astrocyte glycogen and lactate: new insights into learning and memory mechanisms. *Glia* 66:1244–1262.
- Araque A, Parpura V, Sanzgiri RP, Haydon PG (1999) Tripartite synapses: glia, the unacknowledged partner. *Trends Neurosci* 22:208–215.
- Araque A, Carmignoto G, Haydon PG (2001) Dynamic signaling between astrocytes and neurons. *Annu Rev Physiol* 63:795–813.
- Araque A, Carmignoto G, Haydon PG, Oliet SHR, Robitaille R, Volterra A (2014) Gliotransmitters travel in time and space. *Neuron* 81:728–739.
- Berg S, Kutra D, Kroeger T, Straehle CN, Kausler BX, Haubold C, Schiegg M, Ales J, Beier T, Rudy M, Eren K, Cervantes JI, Xu B, Beuttenmueller F, Wolny A, Zhang C, Koethe U, Hamprecht FA, Kreshuk A (2019) ilastik: interactive machine learning for (bio)image analysis. *Nat Methods* 16:1226–1232.
- Bezzi P, Volterra A (2001) A neuron-glia signalling network in the active brain. *Curr Opin Neurobiol* 11:387–394.
- Chen BK, Murawski NJ, Cincotta C, McKissick O, Finkelstein A, Hamidi AB, Merfeld E, Doucette E, Grella SL, Shpkayte M, Zaki Y, Fortin A, Ramirez S (2019) Artificially enhancing and suppressing hippocampus-mediated memories. *Curr Biol* 29:1885–1894.e4.
- Cho WH, Noh K, Lee BH, Barcelon E, Jun SB, Park HY, Lee SJ (2022) Hippocampal astrocytes modulate anxiety-like behavior. *Nat Commun* 13:6536.
- Corkrum M, Covelo A, Lines J, Bellocchio L, Pisansky M, Loke K, Quintana R, Rothwell PE, Lujan R, Marsicano G, Martin ED, Thomas MJ, Kofuji P, Araque A (2020) Dopamine-evoked synaptic regulation in the nucleus accumbens requires astrocyte activity. *Neuron* 105:1036–1047.e5.
- Covelo A, Araque A (2018) Neuronal activity determines distinct gliotransmitter release from a single astrocyte. *Elife* 7:e32237.
- Cui G, Jun SB, Jin X, Luo G, Pham MD, Lovinger DM, Vogel SS, Costa RM (2014) Deep brain optical measurements of cell type-specific neural activity in behaving mice. *Nat Protoc* 9:1213–1228.
- di Castro MA, Chuquet J, Liaudet N, Bhaukaurally K, Santello M, Bouvier D, Tiret P, Volterra A (2011) Local Ca²⁺ detection and modulation of synaptic release by astrocytes. *Nat Neurosci* 14:1276–1284.
- Durkee CA, Covelo A, Lines J, Kofuji P, Aguilar J, Araque A (2019) Gi/o protein-coupled receptors inhibit neurons but activate astrocytes and stimulate gliotransmission. *Glia* 67:1076–1093.
- Eichenbaum H, Schoenbaum G, Young B, Bunsey M (1996) Functional organization of the hippocampal memory system. *Proc Natl Acad Sci U S A* 93:13500–13507.
- Fan XC, Ma CN, Song JC, Liao ZH, Huang N, Liu X, Ma L (2021) Rac1 signaling in amygdala astrocytes regulates fear memory acquisition and retrieval. *Neurosci Bull* 37:947–958.
- Fellin T, Pascual O, Gobbo S, Pozzan T, Haydon PG, Carmignoto G (2004) Neuronal synchrony mediated by astrocytic glutamate through activation of extrasynaptic NMDA receptors. *Neuron* 43:729–743.
- Gao V, Suzuki A, Magistretti PJ, Lengacher S, Pollonini G, Steinman MQ, Alberini CM (2016) Astrocytic β2-adrenergic receptors mediate hippocampal long-term memory consolidation. *Proc Natl Acad Sci U S A* 113:8526–8531.
- Gore F, Schwartz EC, Brangers BC, Aladi S, Stujenske JM, Likhtik E, Russo MJ, Gordon JA, Salzman CD, Axel R (2015) Neural representations of

- unconditioned stimuli in basolateral amygdala mediate innate and learned responses. *Cell* 162:134–145.
- Gunaydin LA, Grosenick L, Finkelstein JC, Kauvar IV, Fenno LE, Adhikari A, Lamme S, Mirzabekov JJ, Airan RD, Zalocusk KA, Tye KM, Anikeeva P, Malenka RC, Deisseroth K (2014) Natural neural projection dynamics underlying social behavior. *Cell* 157:1535–1551.
- Grella SL, Fortin AH, McKissick O, Leblanc H, Ramirez S (2020) Odor modulates the temporal dynamics of fear memory consolidation. *Learn Mem* 27:150–163.
- Han JH, Kushner SA, Yiu AP, Hsiang HL, Buch T, Waisman A, Bontempi B, Neve RL, Frankland PW, Josselyn SA (2009) Selective erasure of a fear memory. *Science* 323:1492–1496.
- Haydon PG (2001) Glia: listening and talking to the synapse. *Nat Rev Neurosci* 2:185–193.
- Howe M, Ridouh I, Mascaro ALA, Larios A, Azcorra M, Dombeck DA (2019) Coordination of rapid cholinergic and dopaminergic signaling in striatum during spontaneous movement. *Elife* 8:e44903.
- Jean-Richard-dit-Bressel P, Clifford CWG, McNally GP (2020) Analyzing event-related transients: confidence intervals, permutation tests, and consecutive thresholds. *Front Mol Neurosci* 13:14.
- Jimenez JC, Berry JE, Lim SC, Ong SK, Kheirbek MA, Hen R (2020) Contextual fear memory retrieval by correlated ensembles of ventral CA1 neurons. *Nat Commun* 11:3492.
- Kim J, Pignatelli M, Xu S, Itohara S, Tonegawa S (2016) Antagonistic negative and positive neurons of the basolateral amygdala. *Nat Neurosci* 19:1636–1646.
- Koizumi S, Fujishita K, Inoue K (2005) Regulation of cell-to-cell communication mediated by astrocytic ATP in the CNS. *Purinergic Signal* 1:211–217.
- Kol A, Adamsky A, Groysman M, Kreisel T, London M, Goshen I (2020) Astrocytes contribute to remote memory formation by modulating hippocampal-cortical communication during learning. *Nat Neurosci* 23:1229–1239.
- Lei Z, Xie L, Li CH, Lam YY, Ramkrishnan AS, Fu Z, Zeng X, Liu S, Iqbal Z, Li Y (2022) Chemogenetic activation of astrocytes in the basolateral amygdala contributes to fear memory formation by modulating the amygdala and prefrontal cortex communication. *Int J Mol Sci* 23:6092.
- Li Y, Li L, Wu J, Zhu Z, Feng X, Qin L, Zhu Y, Sun L, Liu Y, Qiu Z, Duan S, Yu YQ (2020) Activation of astrocytes in the hippocampus decreases fear memory through adenosine A1 receptors. *Elife* 9:e57155.
- Liao Z, Tao Y, Guo X, Cheng D, Wang F, Liu X, Ma L (2017) Fear conditioning downregulates rac1 activity in the basolateral amygdala astrocytes to facilitate the formation of fear memory. *Front Mol Neurosci* 10:396.
- Lin Z, You F, Li T, Feng Y, Zhao X, Yang J, Yao Z, Gao Y, Chen JF (2022) Entrainment of astrocytic and neuronal Ca²⁺ population dynamics during information processing of working memory in mice. *Neurosci Bull* 38:474–488.
- Lines J, Martin ED, Kofuji P, Aguilar J, Araque A (2020) Astrocytes modulate sensory-evoked neuronal network activity. *Nat Commun* 11:3689.
- Liu J, Totty MS, Melissari L, Bayer H, Maren S (2022) Convergent coding of recent and remote fear memory in the basolateral amygdala. *Biol Psychiatry* 91:832–840.
- Liu X, Ramirez S, Pang PT, Puryear CB, Govindarajan A, Deisseroth K, Tonegawa S (2012) Optogenetic stimulation of a hippocampal engram activates fear memory recall. *Nature* 484:381–385.
- Lopes G, Bonacchi N, Frazão J, Neto JP, Atallah BV, Soares S, Moreira L, Matias S, Itskov PM, Correia PA, Medina RE, Calcaterra L, Dreosti E, Paton JJ, Kampff AR (2015) Bonsai: an event-based framework for processing and controlling data streams. *Front Neuroinform* 9:7.
- Maren S (1999) Neurotoxic basolateral amygdala lesions impair learning and memory but not the performance of conditional fear in rats. *J Neurosci* 19:8696–8703.
- Maren S, Aharonov G, Fanselow MS (1996) Retrograde abolition of conditional fear after excitotoxic lesions in the basolateral amygdala of rats: absence of a temporal gradient. *Behav Neurosci* 110:718–726.
- Martin-Fernandez M, Jamison S, Robin LM, Zhao Z, Martin ED, Aguilar J, Benneyworth MA, Marsicano G, Araque A (2017) Synapse-specific astrocyte gating of amygdala-related behavior. *Nat Neurosci* 20:1540–1548.
- Mathis A, Mamićanna P, Cury KM, Abe T, Murthy VN, Mathis MW, Bethge M (2018) DeepLabCut: markerless pose estimation of user-defined body parts with deep learning. *Nat Neurosci* 21:1281–1289.
- Parpura V, Basarsky TA, Liu F, Jeftinija K, Jeftinija S, Haydon PG (1994) Glutamate-mediated astrocyte-neuron signalling. *Nature* 369:744–747.
- Perea G, Araque A (2005) Glial calcium signaling and neuron-glia communication. *Cell Calcium* 38:375–382.
- Perea G, Navarrete M, Araque A (2009) Tripartite synapses: astrocytes process and control synaptic information. *Trends Neurosci* 32:421–431.
- Porter JT, McCarthy KD (1997) Astrocytic neurotransmitter receptors *in situ* and *in vivo*. *Prog Neurobiol* 51:439–455.
- Pratt WE, Mizumori SJ (1998) Characteristics of basolateral amygdala neuronal firing on a spatial memory task involving differential reward. *Behav Neurosci* 112:554–570.
- Pryce CR (2018) Comparative evidence for the importance of the amygdala in regulating reward salience. *Curr Opin Behav Sci* 22:76–81.
- Qin H, He W, Yang C, Li J, Jian T, Liang S, Chen T, Feng H, Chen X, Liao X, Zhang K (2020) Monitoring astrocytic Ca²⁺ activity in freely behaving mice. *Front Cell Neurosci* 14:603095.
- Rashid AJ, Yan C, Mercaldo V, Hsiang HL, Park S, Cole CJ, De Cristofaro A, Yu J, Ramakrishnan C, Lee SY, Deisseroth K, Frankland PW, Josselyn SA (2016) Competition between engrams influences fear memory formation and recall. *Science* 353:383–387.
- Redondo RL, Kim J, Arons AL, Ramirez S, Liu X, Tonegawa S (2014) Bidirectional switch of the valence associated with a hippocampal contextual memory engram. *Nature* 513:426–430.
- Sengupta A, Yau JOY, Jean-Richard-dit-Bressel P, Liu Y, Millan EZ, Power JM, McNally GP (2018) Basolateral amygdala neurons maintain aversive emotional salience. *J Neurosci* 38:3001–3012.
- Shelkar GP, Liu J, Dravid SM (2021) Astrocytic NMDA receptors in the basolateral amygdala contribute to facilitation of fear extinction. *Int J Neuropsychopharmacol* 24:907–919.
- Stehberg J, Moraga-Amaro R, Salazar C, Becerra A, Echeverría C, Orellana JA, Bultynck G, Ponsaerts R, Leybaert L, Simon F, Sáez JC, Retamal MA (2012) Release of gliotransmitters through astroglial connexin 43 hemichannels is necessary for fear memory consolidation in the basolateral amygdala. *FASEB J* 26:3649–3657.
- Steinman MQ, Gao V, Alberini CM (2016) The role of lactate-mediated metabolic coupling between astrocytes and neurons in long-term memory formation. *Front Integr Neurosci* 10:10.
- Trouche S, Perestenko PV, van de Ven GM, Bratley CT, McNamara CG, Campo-Urriza N, Black SL, Reijmers LG, Dupret D (2016) Recoding a cocaine-place memory engram to a neutral engram in the hippocampus. *Nat Neurosci* 19:564–567.
- Tsunematsu T, Sakata S, Sanagi T, Tanaka KF, Matsui K (2021) Region-specific and state-dependent astrocyte Ca²⁺ dynamics during the sleep-wake cycle in mice. *J Neurosci* 41:5440–5452.
- Van Den Herrewegen Y, Sanderson TM, Sahu S, de Bundel D, Bortolotto ZA, Smolders I (2021) Side-by-side comparison of the effects of Gq- and Gi-DREADD-mediated astrocyte modulation on intracellular calcium dynamics and synaptic plasticity in the hippocampal CA1. *Mol Brain* 14:144.
- Volterra A, Meldolesi J (2005) Astrocytes, from brain glue to communication elements: the revolution continues. *Nat Rev Neurosci* 6:626–640.
- Zaki Y, Mau W, Cincotta C, Monasterio A, Odom E, Doucette E, Grella SL, Merfeld E, Shpkayte M, Ramirez S (2022) Hippocampus and amygdala fear memory engrams re-emerge after contextual fear relapse. *Neuropsychopharmacology* 47:1992–2001.
- Zhang X, Li B (2018) Population coding of valence in the basolateral amygdala. *Nat Commun* 9:5195.
- Zhang ZM, Chen S, Liang YZ (2010) Baseline correction using adaptive iteratively reweighted penalized least squares. *Analyst* 135:1138–1146.
- Zhao J, Wang D, Wang JH (2012) Barrel cortical neurons and astrocytes coordinately respond to an increased whisker stimulus frequency. *Mol Brain* 5:12.
- Zheng J, Anderson KL, Leal SL, Shestyuk A, Gulsen G, Mnatsakanian L, Vadera S, Hsu FPK, Yassa MA, Knight RT, Lin JJ (2017) Amygdala-hippocampal dynamics during salient information processing. *Nat Commun* 8:14413.